NASA Technical Memorandum 103729

Cooling of In-Situ Propellant Rocket Engines for Mars Mission

Elizabeth S. Armstrong
Lewis Research Center
Cleveland, Ohio

Corrected Copy

January 1991

NASA

COOLING OF IN-SITU PROPELLANT

ROCKET ENGINES FOR MARS MISSIONS

ELIZABETH S. ARMSTRONG
National Aeronautics and Space Administration
Lewis Research Center
Cleveland, Ohio 44135

ABSTRACT

When contemplating the human exploration of Mars, many scenarios using various propulsion systems have been considered. One propulsion option for a Mars ascent/descent vehicle is multiple high-pressure, pump-fed rocket engines using in-situ propellants, which have been derived from substances available on the Martian surface. The chosen in-situ propellant combination for this analysis is carbon monoxide as the fuel and oxygen as the oxidizer. Both could be extracted from carbon dioxide, which makes up about 96% of the Martian atmosphere.

A pump-fed rocket engine allows for higher chamber pressure than a pressure-fed engine, which in turn results in higher thrust and also higher heat flux in the combustion chamber. The heat flowing through the wall cannot be sufficiently dissipated by radiation cooling and, therefore, a regenerative coolant may be necessary to avoid melting the rocket engine. The two possible fluids for this coolant scheme, carbon monoxide and oxygen, are compared analytically. To determine their heat transfer capability, they are evaluated based upon their heat transfer and fluid flow characteristics. Heat transfer correlations were examined for applicability to each fluid and a correlation was chosen for each

coolant. Implementing the heat transfer correlations into the Rocket Engine Heat Transfer Evaluation Program (REHTEP), the two coolants were compared and the coolant geometries were optimized while considering certain limitations such as temperature and pressure constraints. The pressure drop and hot-gas-side wall temperature results from REHTEP were compared for each coolant channel geometry to determine which fluid was the better coolant under optimum conditions.

The use of carbon monoxide as a coolant results in a lower coolant inlet pressure from the turbopumps and a cooler chamber wall and, hence, a less severe operating condition. Overall, for a given wall temperature, carbon monoxide cooling results in a lower pressure drop than oxygen cooling, under optimum conditions.

NOMENCLATURE

A	area	cm^2
A$_c$	coolant channel area	cm^2
AR	aspect ratio, height-to-width ratio	
A$_t$	throat area	cm^2
C$_f$	thrust coefficient	
C$_p$	specific heat	J/kg-K
$\hat{C}_p$	integrated average specific heat	J/kg-K
C*	characteristic exhaust velocity	m/s
d	diameter	cm
d$_c$	coolant channel diameter	cm
F	thrust level	N
f	friction factor	
f$_{rough}$	friction factor for a rough tube	
f$_{smooth}$	friction factor for a smooth tube	
g$_c$	gravitational constant for earth	kg-m/N-s^2
h	convection heat transfer coefficient	W/m^2-K
I$_{sp}$	specific impulse	s
k	conductivity	W/m-K
k$_b$	conductivity at the mean bulk temperature	W/m-K
k$_w$	conductivity at the wall temperature	W/m-K
L	total length	cm
L$_c$	total length of the combustion chamber	cm
L$_{cv}$	total length of the curved portion of the tube	cm
m$_{bo}$	burnout mass	kg

m_i	initial mass	kg
m_c	mass flowrate	kg/s
N_c	number of cooling channels	
Nu	Nusselt Number	
Nu_{calc}	calculated Nusselt Number	
Nu_{exp}	experimentally determined Nusselt Number	
Nu_r	reduced Nusselt Number, Nu_{exp}/Nu_{calc}	
Nu_0	Nusselt Number at constant physical property conditions	
P	pressure	MPa
P_a	ambient pressure	MPa
P_c	chamber pressure	MPa
P_{cr}	critical pressure	MPa
Pr	Prandtl Number	
Pr_b	Prandtl Number at the mean bulk temperature	
Pr_f	Prandtl Number at the film temperature	
PR	pressure ratio	
R	radius of curvature	cm
r	radius	cm
r_t	throat radius	cm
Re	Reynolds Number	
Re_b	Reynolds Number at the mean bulk temperature	
Re_f	Reynolds Number at the film temeperature	
T	temperature	K
T_b	mean bulk temperature	K
T_w	wall temperature	K
t_s	stay time	s

V	velocity	m/s
v	average specific volume of combustion products	m^3/kg
Vol_c	combustion chamber volume	m^3
x	distance	cm
x_{cv}	distance along the tube from the beginning of the curved portion	cm
w_{bl}	baseline width	cm
z	axial distance along a nozzle	cm

Greek Symbols

γ	specific heat ratio	
ϵ_c	contraction area ratio	
θ_c	chamber contraction angle	
μ	dynamic viscosity	$kg/m^2\text{-}s$
μ_b	dynamic viscosity at the mean bulk temperature	$kg/m^2\text{-}s$
μ_w	dynamic viscosity at the wall temperature	$kg/m^2\text{-}s$
ρ	density	kg/m^3
ρ_b	density at the mean bulk temperature	kg/m^3
ρ_w	density at the wall temperature	kg/m^3
ϕ_{cv}	curvature effect on heat transfer	
ϕ_{en}	entrance effect on heat transfer	
ϕ_{fr}	effect of friction on heat transfer	

TABLE OF CONTENTS

TABLE OF CONTENTS (CONTINUED)

CHAPTER I

INTRODUCTION

The aerospace community is seriously considering human exploration of Mars as part of the future of the space program. Many scenarios for manned missions (ref. 1-7) are being examined, using various propulsion systems. One viable propulsion system is a pump-fed, high-pressure rocket engine using the in-situ propellant combination (propellants extracted from substances available on the Martian surface) of carbon monoxide and oxygen.

A pump-fed, high-pressure rocket engine is reusable and provides high performance. However, it also has a high heat flux, requiring a mechanism to transfer heat from the combustion gases. The simplest method of transferring heat from the combustion gases is radiation cooling to the Martian atmosphere. From the Stefan-Boltzmann Law and assuming blackbody radiation, the chamber wall temperature could reach 6000 K (10,800 R) or above for a throat heat flux of 80 MW/m² (50 BTU/in²-sec), half of the heat flux at the Space Shuttle Main Engine (SSME) throat. Since no known material could withstand such a temperature without melting, the rocket engine will require additional cooling methods. A proposed scheme is conductive heat transfer through the chamber wall and convective heat transfer into a regenerative coolant.

The rocket engine could also use film cooling or transpiration cooling. However, these cooling methods would reduce the performance of the engine and, hence, were not considered.

Using an in-situ propellant combination has several advantages over bringing all of the propellants from earth. Although several cargo vehicles, weighing about 149,000 kg each, are initially needed to deliver the propellant processing equipment, no additional trips are necessary (ref. 6). A sample processing plant, weighing about 50,840 kg (ref. 8), could produce a mass of propellants (oxygen and carbon monoxide) equal to the mass of the in-situ propellant production (ISPP) plant in less than 100 days of operation, assuming an oxygen and carbon monoxide production rate of 782 kg per day. With ISPP, the propellants for the return trip do not have to be lifted off the earth's surface, thereby reducing the cost of each launch or reducing the number of launches required (ref. 6). Also, the systems necessary to land the vehicle on Mars are reduced if the additional mass of the propellants for the return trip is not required.

Assuming in-situ propellants, the most likely cooling candidates are the two propellants, carbon monoxide and oxygen, since both fluids will be readily available. Any other coolant, such as liquid hydrogen, would require extra storage tanks and transport from Earth offsetting the previously mentioned advantages of in-situ propellants. To determine their heat transfer capability, these two possible coolants are evaluated for their heat transfer and fluid flow characteristics.

Because the two fluids have different fluid flow and heat transfer characteristics, different cooling channel geometries would allow for the best cooling scheme for each fluid. Therefore, the dimensions of the

cooling channels are evaluated to find the optimum cooling configuration for given structural and fabrication constraints. The engine wall's thermophysical properties, especially the thermal conductivity and melting temperature, constrain the wall temperature. In addition, the combustion chamber wall should be kept in the elastic region to avoid plastic deformation. Other constraints to the coolant channel geometry are the present manufacturing processes and machining operations. The channels also have structural limitations for height and width; they must withstand the thermal and pressure loads imposed upon the chamber wall during combustion.

When determining the coolant channel geometry, the pressure losses in the channels are also an important consideration. The coolant pressure drop is limited by the projected pumping capability of turn-of-the-century turbopumps, about 46.0 MPa (6670 psi). Allowing for pressure losses in the lines and the injector, the maximum coolant inlet pressure is 42.0 MPa (6090 psia). For comparison, the coolant inlet pressure for the SSME is 41.2 MPa (5978 psia).

A chamber pressure of 22.0 MPa (3200 psia) is assumed for maximum performance while staying within the limitations of the present injector and rocket chamber technology. At such a high chamber pressure, the only feasible engine cycles are the gas generator cycle and the staged combustion cycle. To limit the complexity of the system, a gas generator cycle was chosen. Figure 1 shows a gas generator cycle with the fuel as the regenerative coolant. The cycle would be very similar if the oxidizer is used for combustion chamber cooling. To insure stable combustion in the combustion chamber, a 15% pressure drop is necessary across the injector. In the gas generator cycle, the fluid is

pressurized in the pump section of the turbopump and then flows through the coolant passages. Upon exiting the coolant passages, the fluid flows to the combustion chamber via the injector. Hence, a minimum coolant exit pressure is 25.4 MPa (3690 psia).

The properties of the combustion gases and the optimum expansion area ratio are determined from the Complex Chemical Equilibrium Composition (CEC) Program (ref. 9). The Rao Method of Optimization is used to calculate the optimum nozzle for the thrust chamber for a given expansion area ratio and throat diameter (ref. 10). The combustion chamber dimensions are calculated from general rocket engine design equations (ref. 11).

The Rocket Engine Heat Transfer Evaluation Program (REHTEP) is used for screening coolant channel geometries. In REHTEP, one-dimensional equilibrium properties are calculated for the combustion gases and one-dimensional heat transfer assumptions are made for the chamber wall. The pressure drop and hot-gas-side wall temperature results from REHTEP are compared for each coolant channel geometry to determine the optimum configuration for each of the two fluids, carbon monoxide and oxygen.

Figure 2 shows the relationship between the various computer programs used in this analysis. As can be seen, the CEC output is used as input to the Rao program. The Rao program output is then used as input to the REHTEP, while the CEC is integrated as a subroutine for the hot-gas-side calculations. The FLUID program (ref. 12) is also integrated into REHTEP to obtain coolant properties.
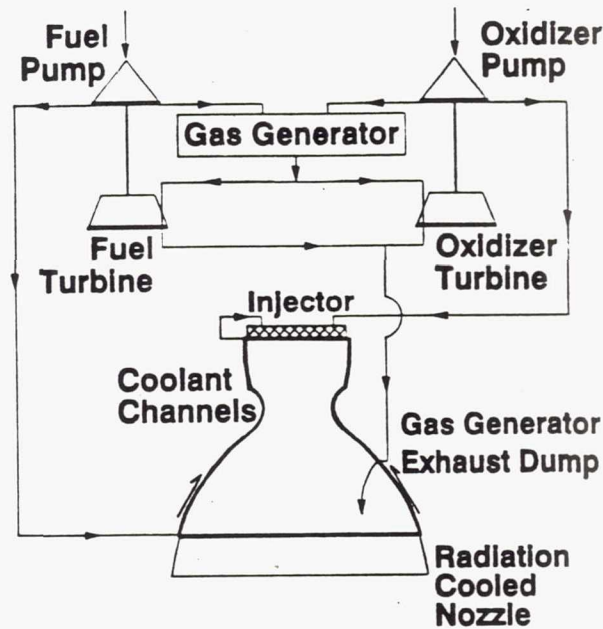
Figure 1.   Gas Generator Cycle with the Fuel as the Regenerative
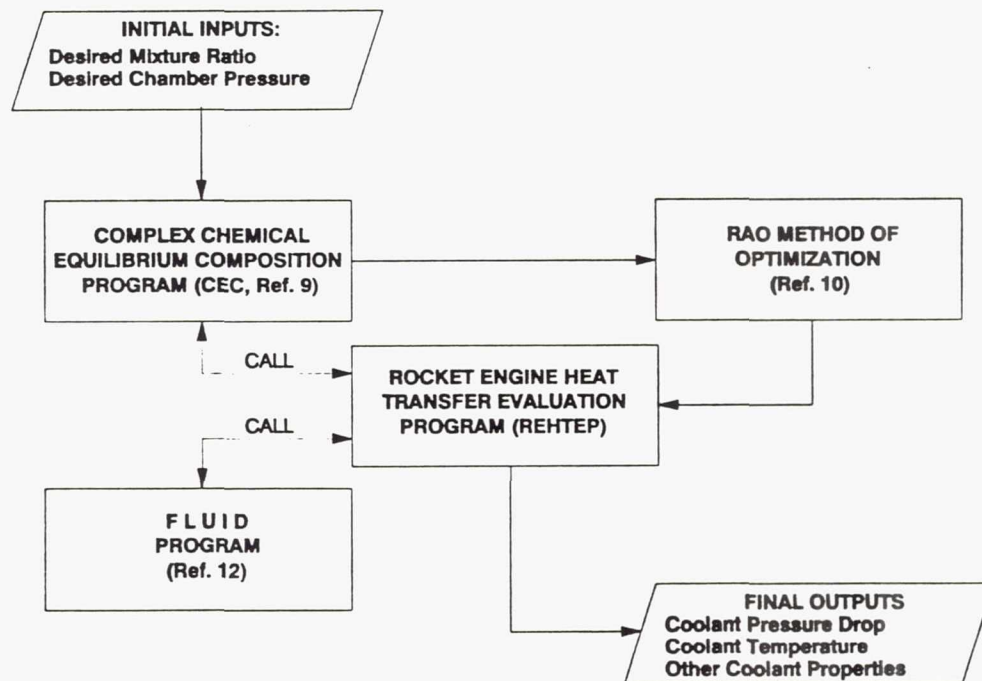   Coolant.

Figure 2.   Block Diagram of the Interaction Between the Various
            Computer Programs Used in This Analysis.

CHAPTER II

BACKGROUND

NASA has studied the Mars atmosphere and surface extensively through the unmanned Mariner and Viking programs, and is now considering a manned program to Mars. Various scenarios for manned missions to Mars have been contemplated (ref. 1), the first serious investigation being Wernher Von Braun's in 1953 (ref. 2). Subsequent publications have considered various propulsion systems and many different vehicle configurations (ref. 3 - 7). Among the most attractive propulsion fuel options are in-situ propellants. In-situ propellants for a Mars ascent/descent vehicle can result in lower earth launch mass, up to 30% over a 10 mission or 20-year period (ref. 5), and can result in cost savings due to the decrease in the number of payloads necessary for the Mars Mission when compared with bringing all the propellants from earth (ref. 6).

According to Ramohalli et al. (ref. 13) there are three in-situ propellant production (ISPP) concepts that are feasible:

1) producing only oxygen at Mars and bringing the fuel from Earth,

2) producing carbon monoxide as the fuel and oxygen as the oxidizer,

3) producing methane as the fuel and oxygen as the oxidizer.

The first and third concepts require that all or some of the fuel be brought to Mars from Earth. The major advantage of the second concept is that both oxygen and carbon monoxide can be obtained from carbon dioxide, which makes up about 95% of the Mars atmosphere and is the one thoroughly known and readily available Martian resource.

A number of reports have been published describing ISPP systems (ref. 5, 8, 13 - 17). Lawton and Frisbee (ref. 8, 16, 17) give a very thorough explanation of the basic physics and chemistry of the system used to obtain oxygen from carbon dioxide. The process begins by filtering the Martian atmosphere to remove dust particles and then pumping the atmospheric gases into a reaction cell where they are heated so that O_2 can be dissociated from the CO_2. The O_2 is extracted from the gas mixture using a solid zirconia electrolyte. The electrolyte has the ability to conduct electricity by ionic rather than by electronic conduction. When a voltage is applied across the zirconia, oxygen near the cathode is reduced to O^- ions which migrate to the anode where the O^- ions surrender their electrons and recombine as O_2 gas (ref. 16). The remaining gases are then vented. The vented gases can be chilled to extract CO, which has a lower boiling point than CO_2, for use as the rocket fuel (ref. 8). Lawton (ref. 16) estimates that to produce 10 kg of O_2/day in this manner requires 1400 amps of current through the zirconia membrane. A small nuclear power plant could easily produce the necessary current without extensive equipment or fuel requirements. The entire in-situ propellant production system could be sent on an unmanned cargo vehicle and arrive at Mars prior to the manned mission (ref. 18).

Several Mars ascent/descent vehicle configurations have been investigated as described by Cordell (ref. 1). Figure 3 shows a possible

space vehicle designed to leave low Earth orbit (LEO) and arrive at Mars using an opposition type trajectory with chemical propulsion and no aerobraking assumptions. The Mars descent/ascent portion of the vehicle, which would weigh approximately 60,350 kg, including propellant, is shown in more detail in Figure 4. The habitat and laboratory modules would weigh approximately 60,630 kg (ref. 6, 18). Reference 5 assumes an ascent cargo weight of 0.14 M tons (140 kg), assuming the vehicle would bring some cargo from Mars back to Earth. The Mars ascent/descent vehicle engines will be required to lift this mass through the Martian atmosphere and to overcome the Mars gravitational force of .38 g.

The engines would also need to lift the vehicle to overcome the ascent delta V requirement.[1] The delta V requirement for ascending from Mars varies from a minimum of 3.9 km/s to a typical value of 6.0 km/s to reach an elliptical orbit (ref. 5). Because the specific impulse for the $CO-O_2$ propellant combination is only 245-300 seconds (ref. 19), a large amount of propellant is needed to meet the delta V requirement. Since carbon dioxide is plentiful in the Martian atmosphere, these propellants are readily available. However, they will require larger tanks than other chemical propellant combinations, such as LO_2-LH_2, and the initial mass will therefore be higher. Taking into account all these considerations, three engines capable of delivering 445 kN (100,000 lbf)

---

[1] The delta V, or change in vehicle velocity, is defined as

$$delta\ V = g_e * I_{sp} (ln\ m_i/m_{bo})$$

where g_e is the acceleration due to gravity at the earth's surface, I_{sp} is the specific impulse of the rocket engine, m_i is the initial mass of the vehicle, and m_{bo} is the mass at the end of the thrust period (the burnout mass). The above equation, commonly referred to as the rocket equation, takes into account the variation in vehicle weight during flight due to the consumption of propellant so that the velocity of the vehicle can be determined (ref.20, pp.322-323).
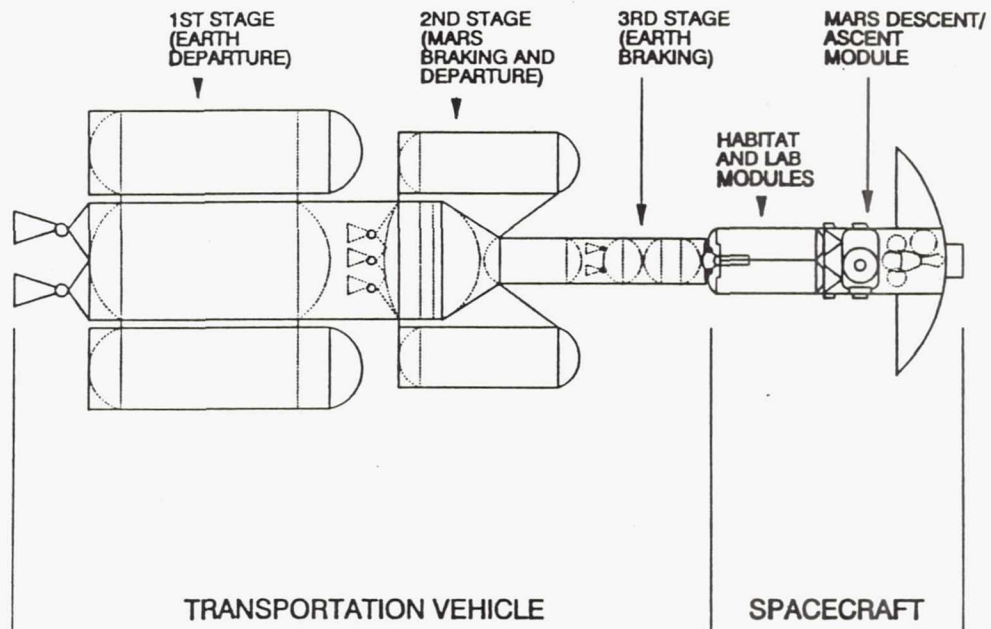
Figure 3.   Space Vehicle for Manned Mars Mission.
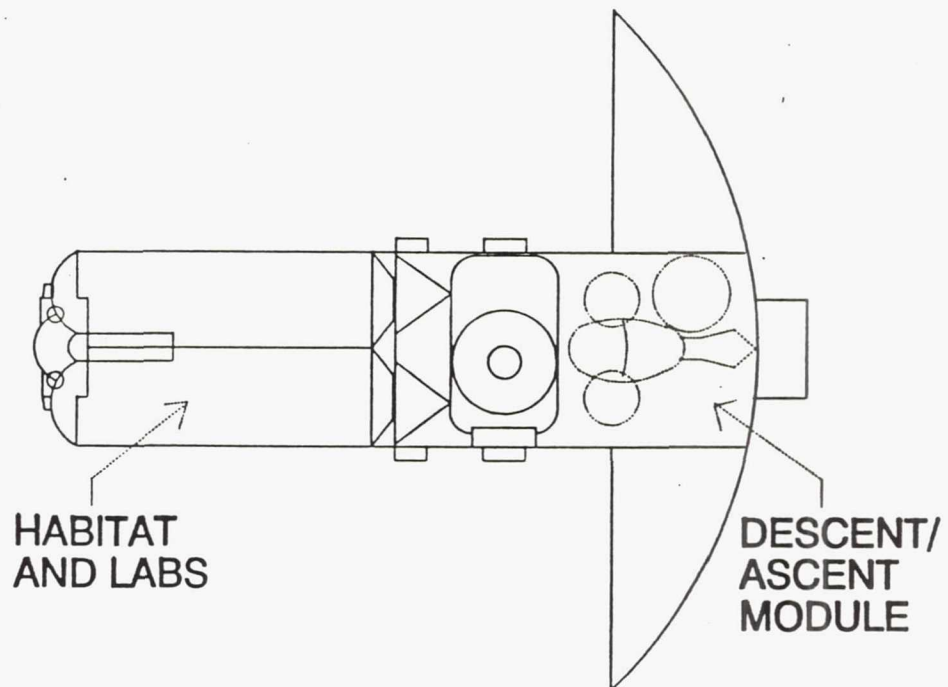
Figure 4.   Baseline Mars Descent/Ascent Vehicle.

of thrust should be sufficient for the vehicle to reach an elliptical orbit for trans-Earth injection (ref. 6).

To deliver 445 kN of thrust and 245-300 seconds of specific impulse, a rocket engine thrust chamber will require a high chamber pressure and a high area ratio nozzle. A high chamber pressure will result in a high heat flux through the chamber walls. At a chamber pressure of 22.1 MPa (3200 psi), the heat flux at the throat could reach more than 80 MW/m^2 (50 Btu/in.^{2} sec) which is more heat than could be dissipated through radiation heat transfer alone. Therefore, other types of cooling must be considered, such as ablative cooling or regenerative cooling. These high heat fluxes could be dissipated through ablative cooling if the engine burn time is short and there is no need for reusability of the engine. If the engine burn time is more than several minutes or the engines are required to be reusable, the best cooling method is regenerative cooling through cooling channels in the chamber walls.

To determine the best regenerative coolant for this application, carbon monoxide or oxygen, their thermophysical properties are compared and their fluid flow and heat transfer characteristics are evaluated. Also, various heat transfer cooling correlations are investigated for evaluating the heat transfer characteristics of the two coolants.

CHAPTER III

Thermophysical Properties of Oxygen and Carbon Monoxide

In an effort to evaluate the fluid flow and heat transfer characteristics of oxygen and carbon monoxide, their thermophysical properties are compared. All the property values were generated using the GASPLUS code (ref. 21) which calculates properties for a number of pure fluids and mixtures. The GASPLUS code has an accuracy of 3% of reported National Institute of Standards and Technology (NIST) pure fluid data. A 3% accuracy is very good for a fluid property code and is considered adequate for the comparison of carbon monoxide and oxygen thermophysical properties. The thermophysical properties used to evaluate the fluid flow and heat transfer characteristics of a fluid are the density (ρ), the specific heat (C_P), the thermal conductivity (k), and the dynamic viscosity (μ).

These properties were first evaluated at the critical temperature and pressure, where the fluid is considered a vapor. The critical pressure for oxygen and carbon monoxide are calculated from the NIST critical temperature using the pure fluid routines in the GASPLUS code; these properties are given in Table I. Second, the properties were normalized with respect to the critical values and then the properties are nondimensionally compared. This procedure allows for a

11

Table I. Critical Properties of Oxygen and Carbon Monoxide (as
          calculated using GASPLUS)

	Oxygen	Carbon Monoxide
Temperature (K)	154.6	132.9
Pressure (MPa)	5.045	3.494
Density (kg/m³)	498.8	382.1
Dynamic Viscosity (kg/m-s)	308.7×10^{-7}	257.5×10^{-7}
Thermal Conductivity (W/m-K)	13.38×10^{-6}	12.64×10^{-6}
Specific Heat (kJ/kg-K)	4.150	29.07
Prandtl Number	9.57	4.57

nondimensional comparison of the fluids. Due to the differences in the critical pressure and temperatures, it is difficult to compare the actual values of the thermophysical properties to determine relative fluid flow and heat transfer characteristics. Third, the thermophysical properties of oxygen and carbon monoxide were plotted at different pressure ratios (the actual pressure divided by the critical pressure) as a function of the temperature ratio (the actual temperature divided by the critical temperature). A subcritical pressure ratio, critical pressure, and several supercritical pressure ratios were chosen to show the variations and similarities in the thermophysical properties in each region. The supercritical pressure region is generally used for rocket engine cooling applications to avoid the possibility of two phase flow in the cooling channels. The property ratios plotted are shown in Figure 5 through 12. The plots are described and compared in detail below. The actual and normalized values for the thermophysical properties are given in Appendix A.

Density Comparison

The normalized densities for oxygen and carbon monoxide are shown as a function of normalized temperature in Figures 5 and 6. In Figure 5, the normalized density of carbon monoxide is 8% less than the oxygen normalized density at supercritical temperatures (at temperature ratios above one). At subcritical temperatures, the carbon monoxide value is roughly 10% less than that of oxygen. These same trends are apparent at critical and supercritical pressure ratios, as shown in Figure 6. As the pressure increases, the normalized densities increase slightly in the subcritical region, while in the supercritical region, both densities increase and continue to be approximately equal. In the near-critical
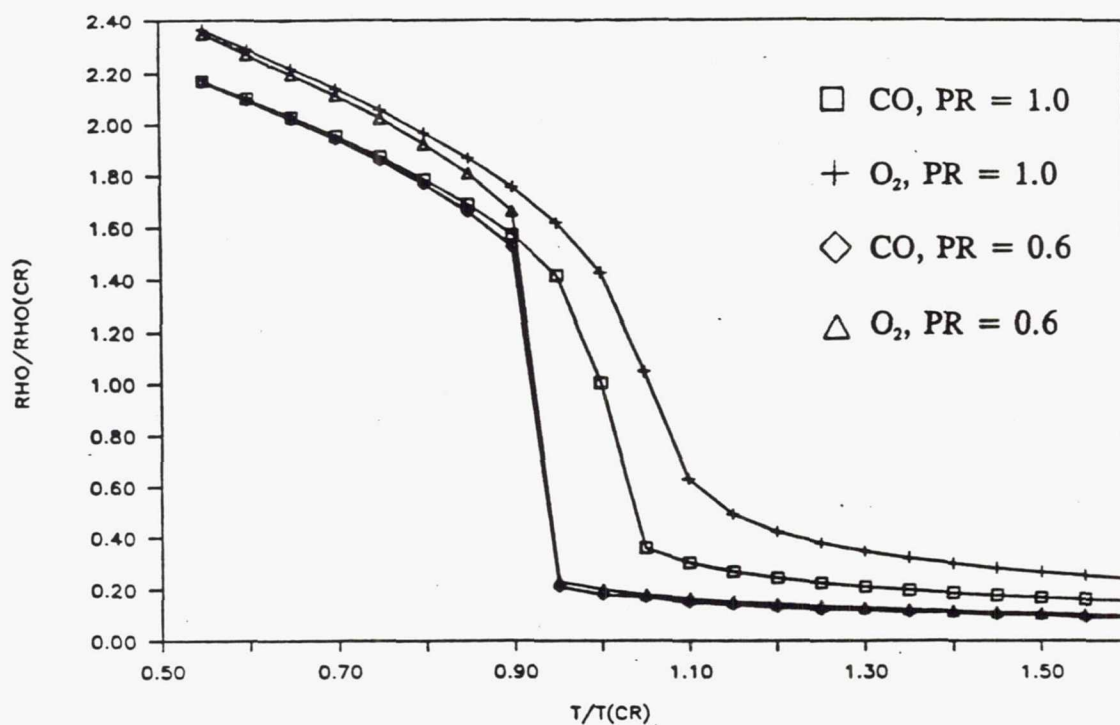
Figure 5.   Comparison of Density Ratios for Various Pressure Ratios
(Subcritical)
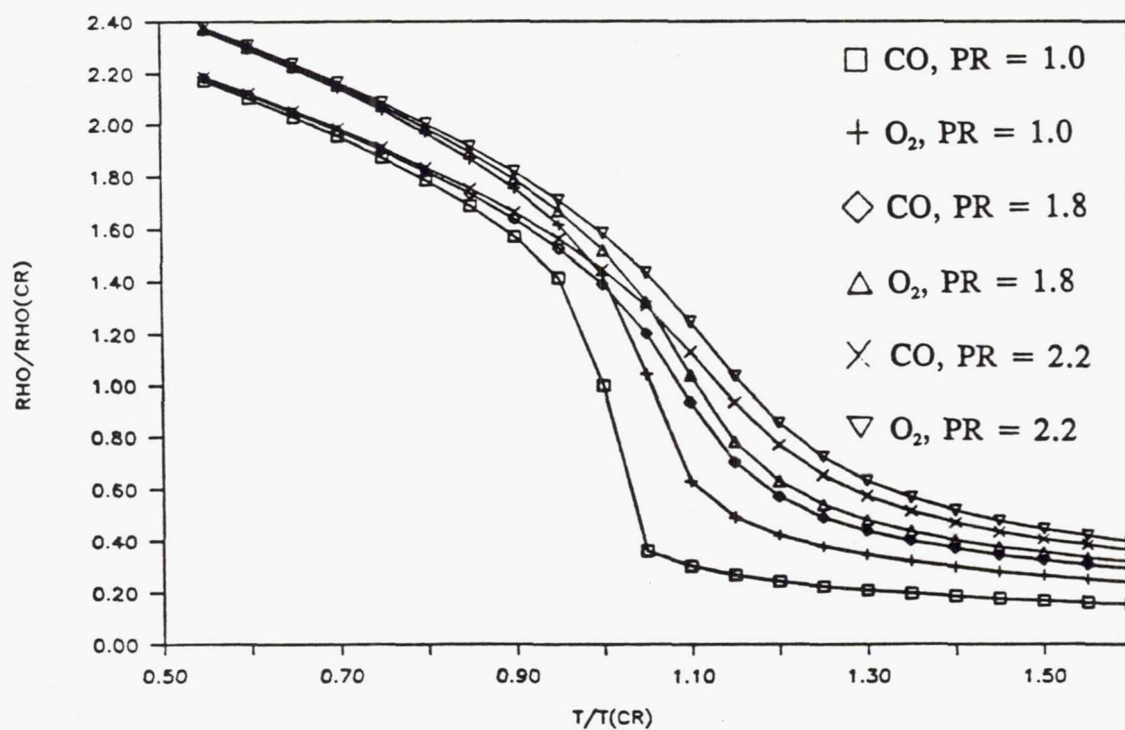
Figure 6.   Comparison of Density Ratios for Various Pressure Ratios
(Supercritical)

temperature region, the curves smooth out and the values for the two gases come within 9% of each another. At the critical pressure and temperature, the density drops suddenly. This transition becomes smoother with increasing pressure ratios. As can be seen, the density does not vary significantly with changes in pressure in the subcritical temperature range.

Viscosity Comparison

The normalized viscosities for oxygen and carbon monoxide as a function of normalized temperature are shown in Figures 7 and 8. Both carbon monoxide and oxygen have low viscosities at pressure ratios of 0.6 (Figure 7) and subcritical temperatures, as would be expected for a liquid. The viscosity rises substantially at the saturation point, which is at the temperature ratio of .92 for both fluids. As is the case with density, the viscosity ratio drops at the critical temperature for a pressure ratio of 1.0 (Figure 7). As the pressure increases (Figure 8), the transition around the critical temperature smoothes out. At all the supercritical pressures, the normalized viscosities for the two fluids are within 8% of each other, with carbon monoxide being higher. The normalized viscosities are almost constant with changes in pressure above the critical pressure.

Thermal Conductivity Comparison

As shown in Figures 9 and 10, the thermal conductivity curves demonstrate trends similar to the density and viscosity curves. At subcritical pressure, the normalized thermal conductivity curves of carbon monoxide and oxygen have the same shape, but the curve for carbon monoxide is roughly 25% higher than the oxygen curve at subcritical temperatures while the oxygen curve is 15% higher at supercritical
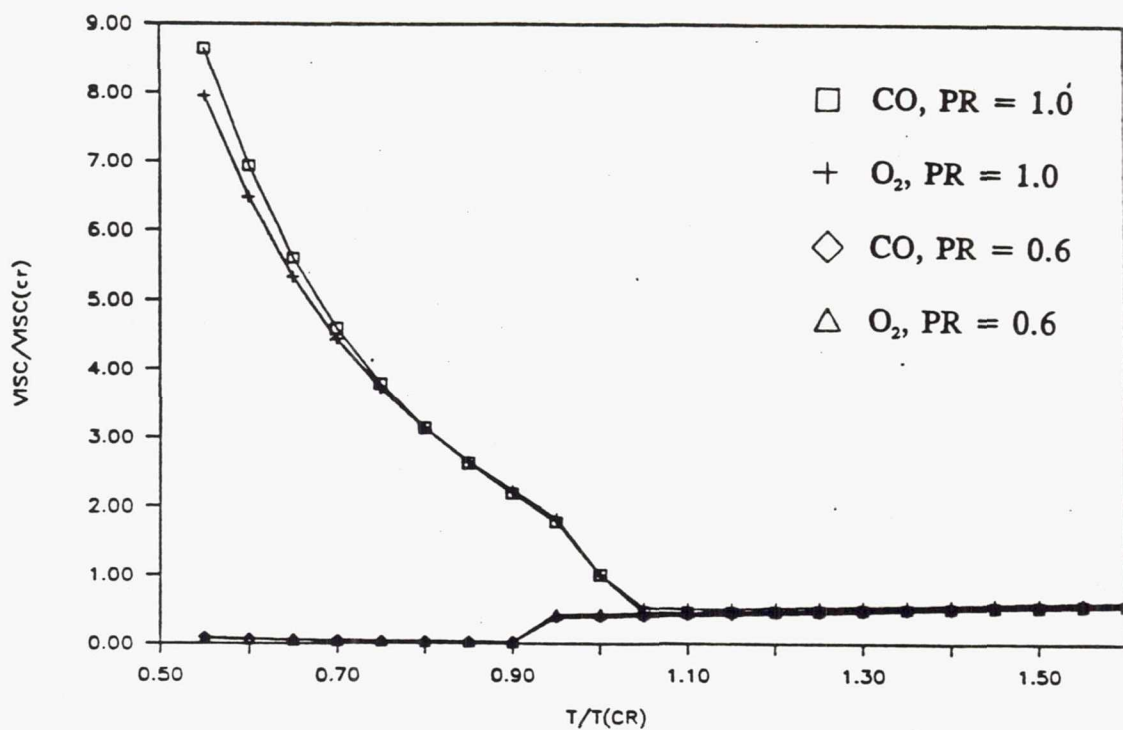
Figure 7.   Comparison of Viscosity Ratios for Various Pressure Ratios
            (Subcritical)

Figure 8.   Comparison of Viscosity Ratios for Various Pressure Ratios
            (Supercritical)

Figure 9.   Comparison of Conductivity Ratios for Various Pressure
Ratios (Subcritical)
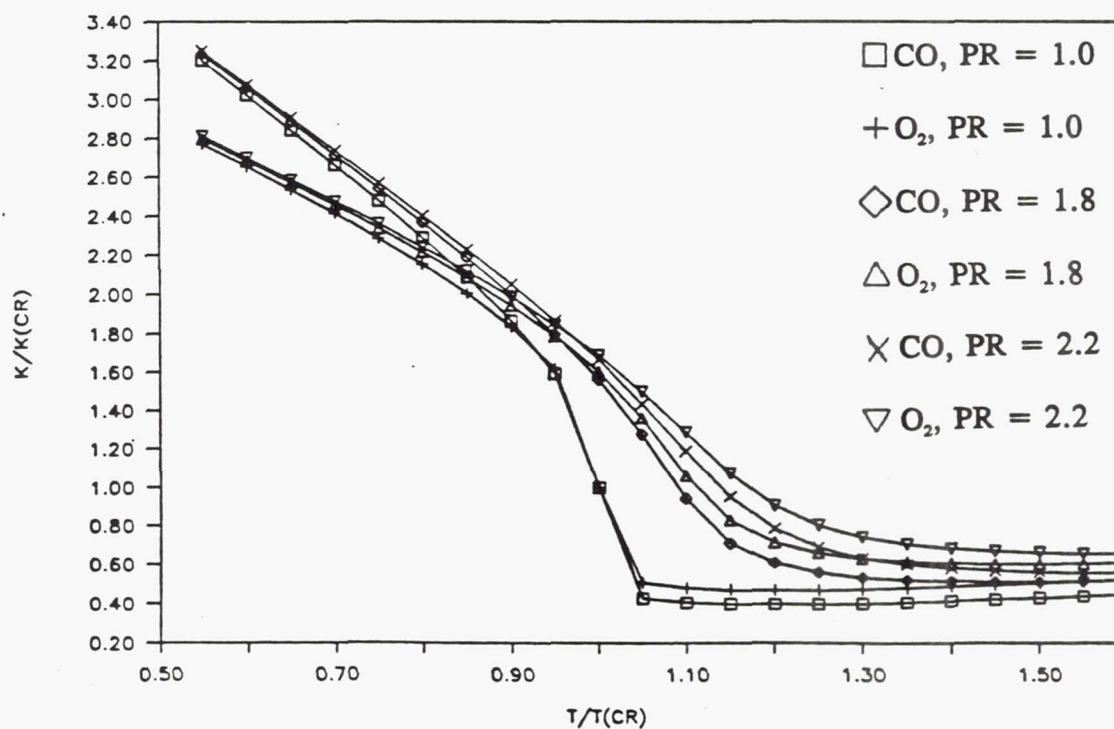
Figure 10.   Comparison of Conductivity Ratios for Various Pressure
Ratios (Supercritical)

temperatures. At and above critical pressure (Figure 10), the thermal conductivity is constant at subcritical temperatures up to a pressure ratio of 1.8. However, at supercritical temperatures the thermal conductivity slightly increases. The two curves cross one another near the critical temperatures for all pressure ratios.

Specific Heat Comparison

Figures 11 and 12 show the normalized specific heats for oxygen and carbon monoxide for the various pressure ratios. Unlike the previous curves, the specific heat ratios of oxygen are significantly greater than those of carbon monoxide. This is due to the critical specific heat of carbon monoxide being much greater than all the other carbon monoxide specific heat values (see Appendix A). The normalized specific heat for oxygen is as much as 6 times that of carbon monoxide at subcritical pressure, as shown in Figure 11. At the critical pressure, the two curves are still significantly separated, only meeting at the critical point (see Figure 11), which they must by definition. As the pressure increases, the peak specific heat shifts toward higher temperatures (Figure 12). Both curves shift approximately the same amount and have the same shape.

Prandtl Number Comparison

As a final comparison, the Prandtl Numbers were calculated for both fluids. The Prandtl Number is defined as

$$Pr = \mu * C_p / k \tag{3.1}$$

The Prandtl Number is shown in Figures 13 and 14 for various pressure ratios. The oxygen values are significantly greater than those for carbon monoxide at the critical pressure. At subcritical pressures, the Prandtl Numbers for the two fluids are very close; the oxygen values are
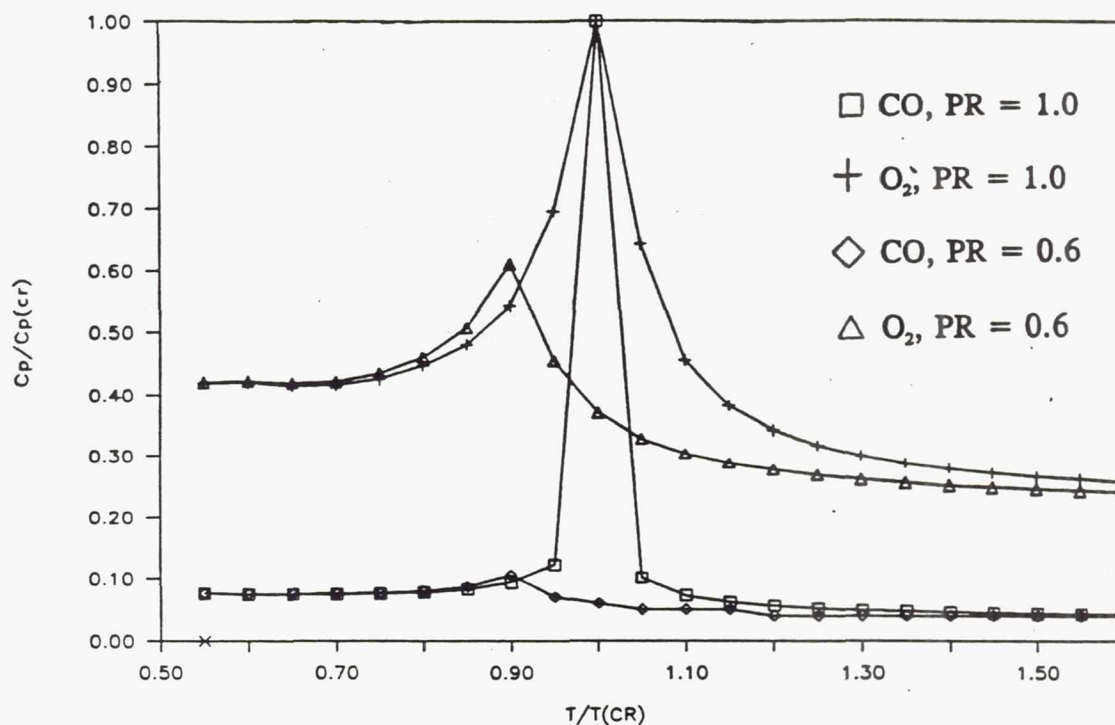
Figure 11. Comparison of Specific Heat Ratios for Various Pressure
Ratios (Subcritical)
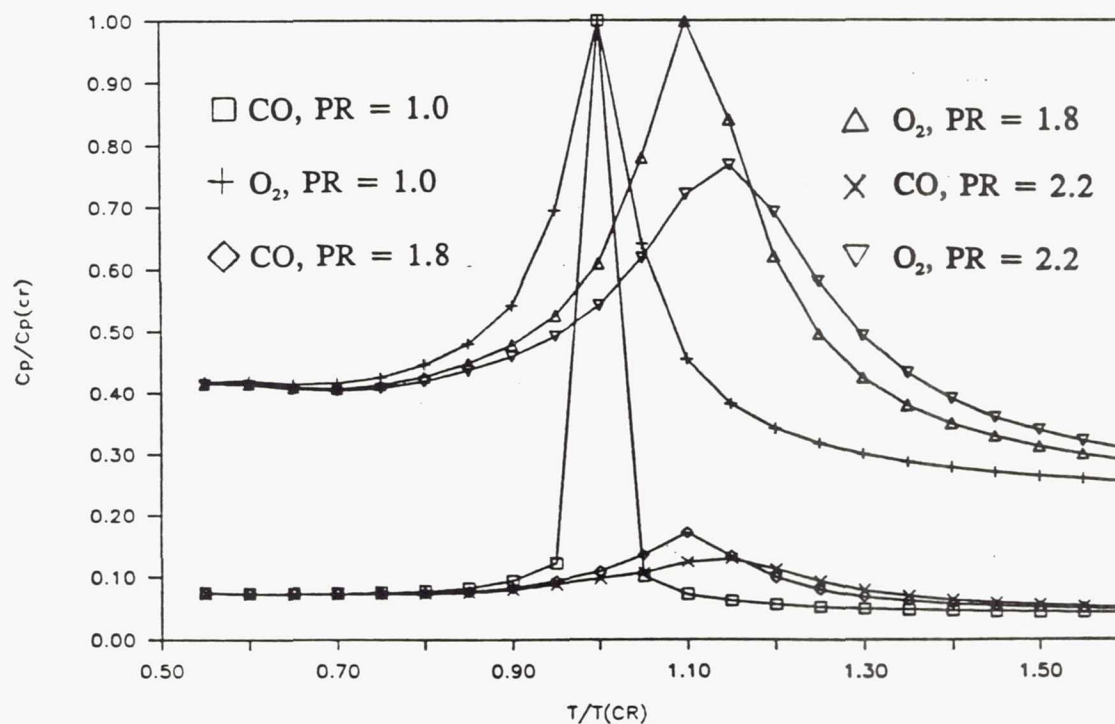
Figure 12. Comparison of Specific Heat Ratios for Various Pressure
Ratios (Supercritical)
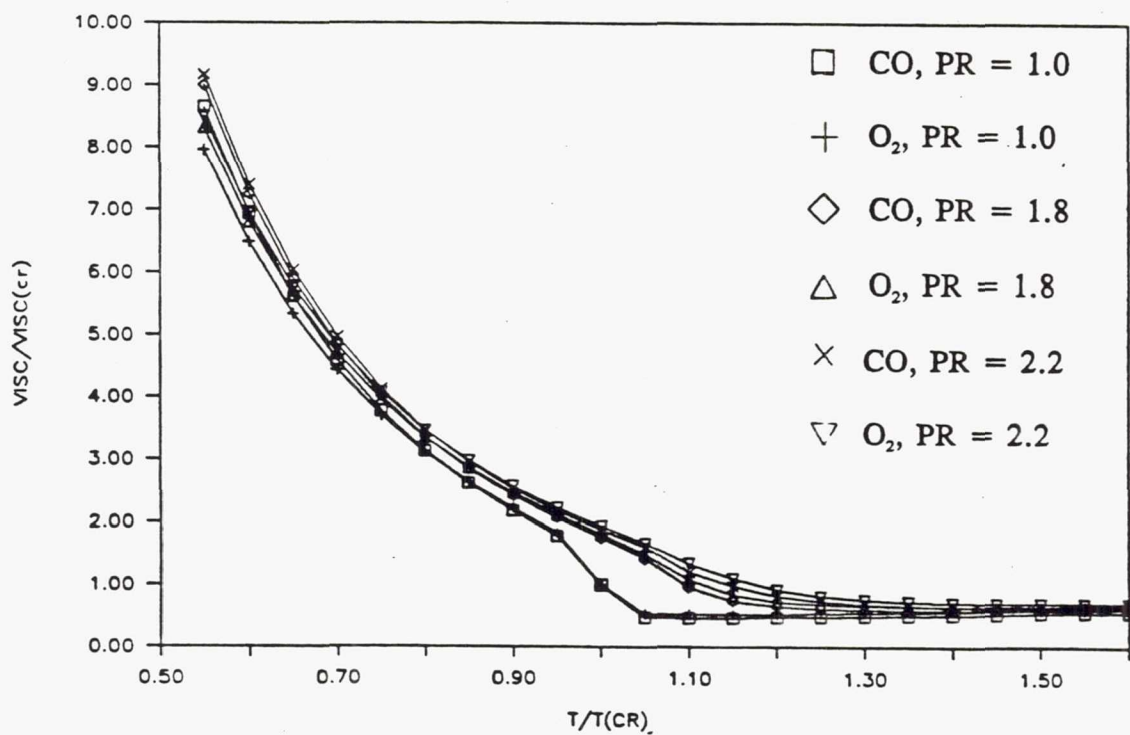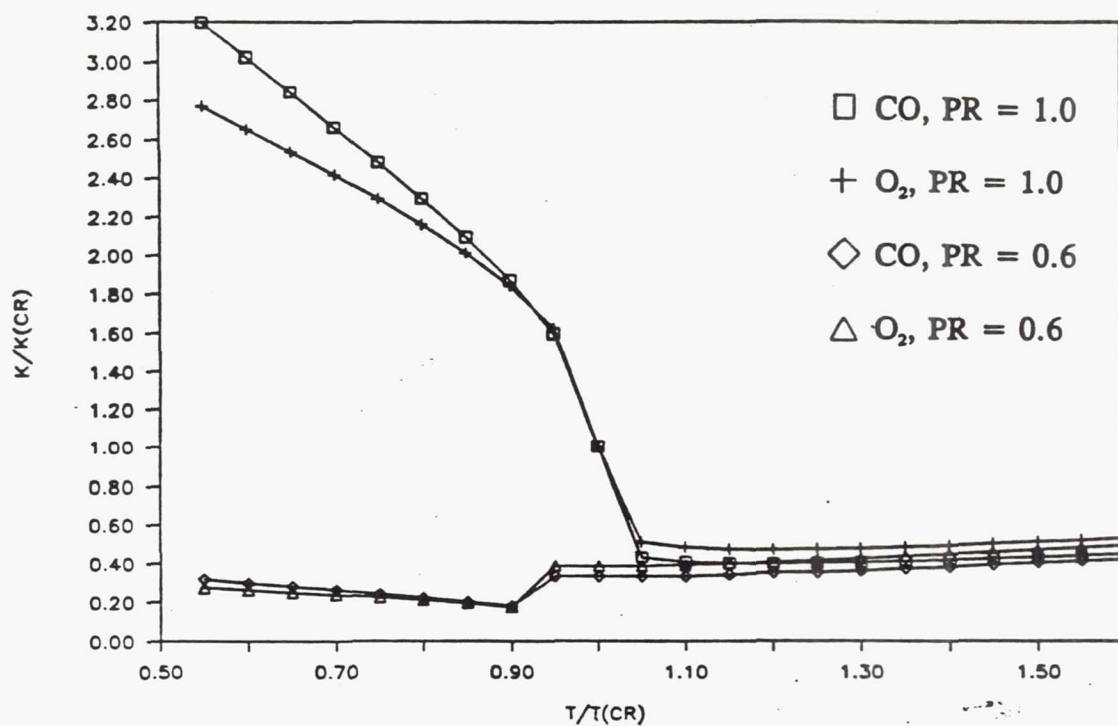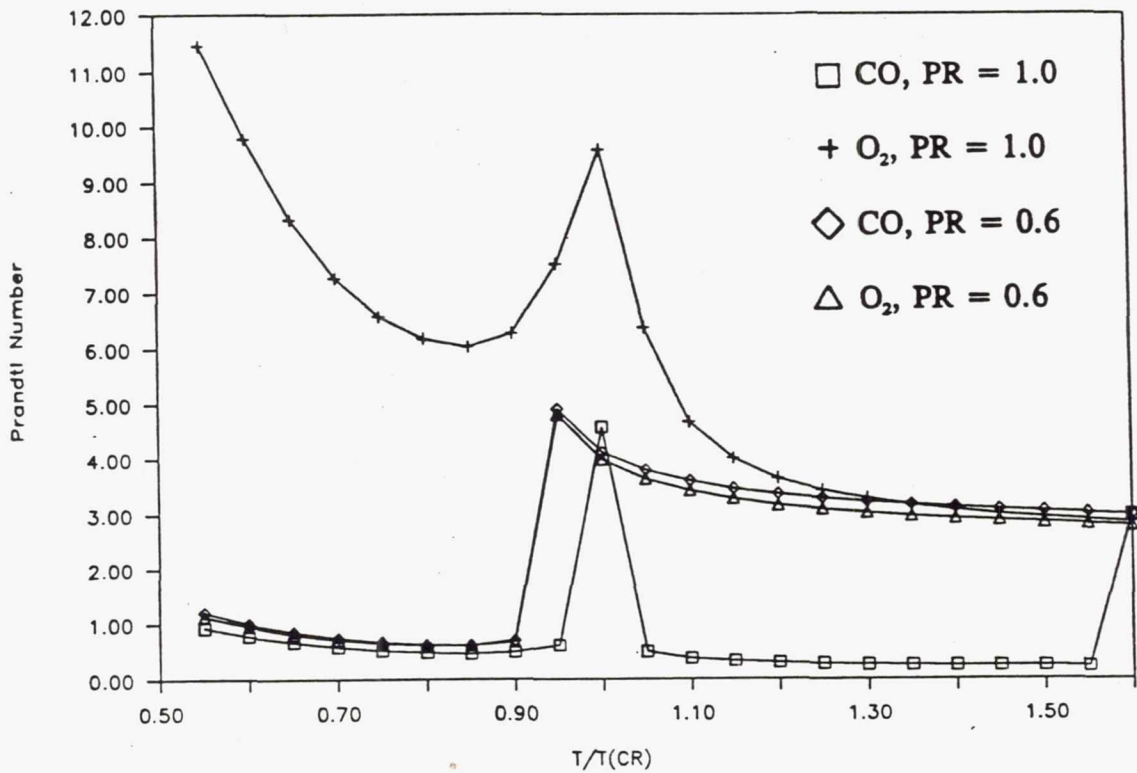
Figure 13.   Comparison of Prandtl Numbers for Various Pressure Ratios
(Subcritical)
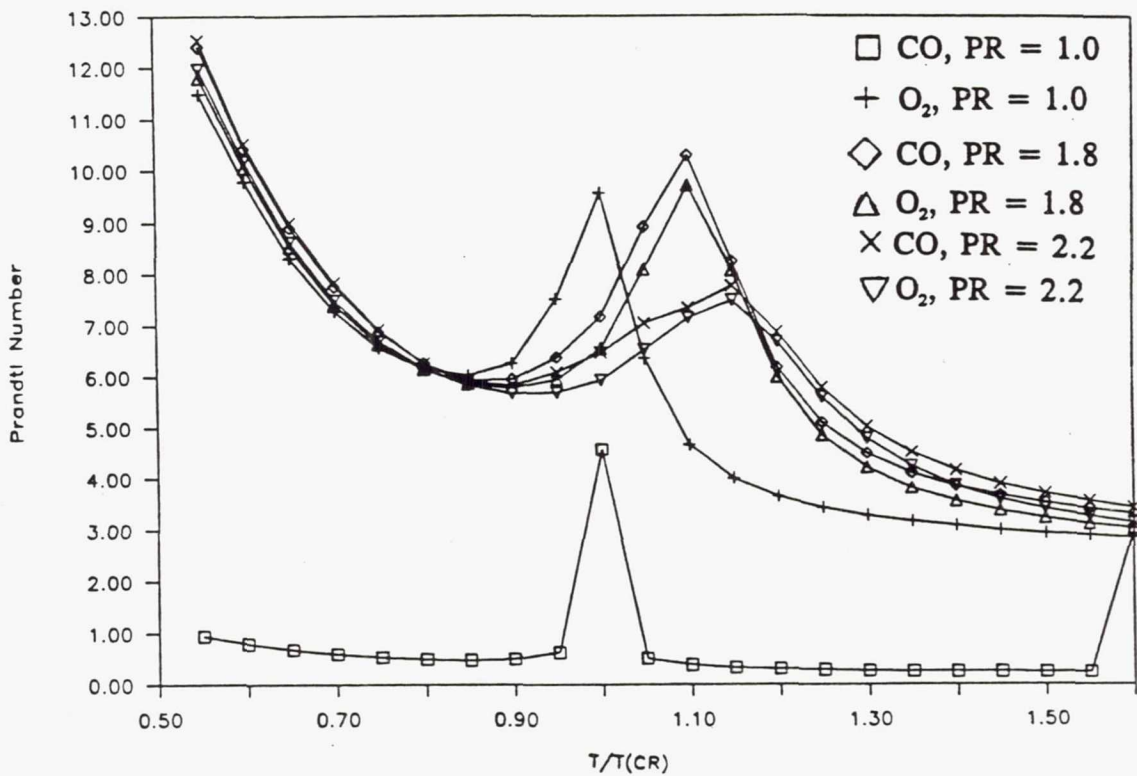
Figure 14.   Comparison of Prandtl Numbers for Various Pressure Ratios
(Supercritical)

only 7% less than those for carbon monoxide (Figure 13). At supercritical pressures, the carbon monoxide values are up to 16% higher than those of oxygen. In the region near the critical temperature, the Prandtl Number curves have distinct peaks, smaller than those for the normalized specific heat curves. The peaks move to the right as the pressure increases, and they also decrease in magnitude, becoming less distinct. These plots show that the Prandtl Number values for the two fluids are similar, and, hence, a determination cannot be made from the Prandtl Number as to which fluid would be the better coolant. The slightly higher Pr values for carbon monoxide may indicate that it would be the better coolant.

Overall Comparison

Figures 5-12 indicate that the density, viscosity, and conductivity of carbon monoxide and oxygen are similar over a wide range of temperatures and pressures. However, the specific heat varies considerably between the two fluids. The Prandtl Number values indicate that it cannot be determined explicitly which fluid is a better coolant. To avoid two phase flow in the cooling channels, only the supercritical pressure range should be examined. A number of heat transfer cooling correlations should be considered and evaluated to predict how carbon monoxide and oxygen will perform in the supercritical pressure region. The coolant pressure region of interest for cooling a rocket engine with a chamber pressure of 22.0 MPa (3200 psia) is 42 MPa (6090 psia) to 22.0 MPa (3200 psia) is the supercritical pressure region. The temperature range would include near-critical and supercritical temperatures.

Therefore, heat transfer cooling correlations for oxygen and carbon monoxide that are applicable to these regions are discussed in the next section.

CHAPTER IV

HEAT TRANSFER CORRELATIONS FOR OXYGEN AND CARBON MONOXIDE

To evaluate the heat transfer characteristics of carbon monoxide and oxygen, the appropriate convective heat transfer equations should be used. First, the most effective heat transfer region should be selected. Second, the appropriate Nusselt Number (Nu) equations should be chosen for the given fluid properties and channel geometry. Finally, the appropriate heat transfer equations should be determined for convective heat transfer analysis.

As mentioned in the previous chapter, the regions of most interest in cooling rocket engines are the near critical temperature, the supercritical temperature, and the supercritical pressure regions. Because of the high chamber pressure, the coolant pressure will always be in the supercritical pressure region and consequently the two phase flow in the coolant channels is not encountered. Petukhov (ref. 22) classifies possible heat transfer regions as a) normal regions; b) regions with diminished heat transfer; and c) regions with enhanced heat transfer. Obviously, regions with diminished heat transfer should be avoided for rocket engine cooling applications. Heat transfer is generally enhanced through turbulence, so a high Reynolds Number (Re) is

23

desirable. Therefore, equations for high Reynolds Number and supercritical pressure are considered in the following analyses.

Carbon Monoxide Heat Transfer Correlations

Since no experimental data is available, it is difficult to determine the best heat transfer correlation for carbon monoxide cooling. For fully developed turbulent flow in smooth tubes, Dittus and Boelter (ref. 23) recommend

$$Nu_0 = .023 \, Re^{0.8} * Pr^{0.4} \tag{4.1}$$

where the coefficient .023 is recommended by McAdams (ref. 24) in place of the .0243 originally given by Dittus and Boelter. This equation is valid for fluids with Prandtl numbers ranging from about .6 to 100 and gives a fair representation of a fluid's heat transfer characteristics, but can be improved upon for a given geometry configuration if enough information is available about the particular application. Petukhov (ref. 22) presents several correlations for constant-property, fully-developed heat-transfer coefficients in pipes. The following equation correlates his results within 10 percent for Prandtl numbers from 0.5 to 2000 and Reynolds numbers from 10^4 to 5×10^6:

$$Nu_0 = \frac{(f/8) \, Re \, Pr}{1.07 + (12.7(f/8)^{1/2}(Pr^{.667} - 1))} \tag{4.2}$$

where

$$f = (1.82 \, \log_{10} Re - 1.64)^{-2}$$

Notter and Sleicher (ref. 25) also presented a correlation for constant physical property fluids in pipes. The following equation correlates

their results within 10 percent for Prandtl numbers from 0.10 to 10^4 and Reynolds numbers from 10^4 to 10^6:

$$Nu_0 = 5 + .015Re^a Pr^b \tag{4.3}$$

where

$$a = 0.88 - 0.24/(4+Pr)$$

and

$$b = 1/3 + 0.5e^{-0.6Pr}$$

When comparing equation (4.2) with equation (4.3), the equations give very similar results, within 9 percent of each other.

If there is a large temperature variation in the flow, there could be a substantial change in the fluid properties across the flow field and constant property correlations would not be applicable. To take property variations into account the bulk properties and wall properties should be included in the Nusselt Number equation

$$Nu = .023 \, Re_b^{0.8} * Pr_b^{0.4} * \left(\frac{\mu_b}{\mu_w}\right)^a * \left(\frac{k_b}{k_w}\right)^b * \left(\frac{\rho}{\rho_w}\right)^c * \left(\frac{\hat{C}_p}{C_p}\right)^d \tag{4.4}$$

Sieder and Tate (ref. 26) recommended the following relation for liquids to take property variations into account:

$$Nu = .023 \, Re_b^{0.8} * Pr_b^{0.33} * \left(\frac{\mu_b}{\mu_w}\right)^{0.14} \tag{4.5}$$

For variable property liquid, Petukhov (ref. 22) recommends equation (4.2) with an additional term:

$$Nu = Nu_0 * \left(\frac{\mu_b}{\mu_w}\right)^n \tag{4.6}$$

where n = 0.11 for heating and 0.25 for cooling. Another consideration is entrance effects which Nusselt (ref. 27) accounted for in the following equation

$$Nu = .036 \, Re^{0.8} * Pr^{0.33} * \left(\frac{d}{L}\right)^{0.55} \tag{4.7}$$

where d is the diameter of the pipe or tube and L is the total length of

the pipe or tube.

Spencer and Rousar (ref. 28) accounted for entrance effects using

$$1 + 2/(L/d)$$

Other entrance effect terms include

$$1 + (A*d)/L \qquad \text{and} \qquad \frac{2.88}{(L/d)^{.325}}$$

where A is the area of the tube at the entrance.

A new correlation has been presented by the authors of references 29 - 31 that takes property variations into account and can be used for any Newtonian fluid with a Prandtl Number ranging from 0.6 to 100. In this heat transfer correlation, the Nusselt Number is given by

$$Nu_r = \frac{Nu_{exp}}{Nu_{calc}} = \phi_{ent} * \phi_{fr} * \phi_{cv} \qquad (4.8a)$$

or

$$Nu_{exp} = Nu_{calc} * \phi_{ent} * \phi_{fr} * \phi_{cv} \qquad (4.8b)$$

where

$$Nu_{calc} = .062 \, Re_f^{0.7} * Pr_f^{0.4}$$

$$\phi_{cv} = (Re_b \, (r/R)^2)^{\pm 0.02} * [1 + \tfrac{1}{2}\sin\{\pi(x_{cv}/(L_{cv} + 15d))^{.5}\}]$$

$$\phi_{fr} = \{1 + B*(Pr_b - 1)\}*F/\{1 + B*(Pr_b*F - 1)\}$$

where

$$B = 1.5/(Pr_b^{1/6} \, Re_b^{1/8})$$

$$F = f_{rough}/f_{smooth}$$

$$f_{smooth} = 0.0778(Re_b)^{-.1021}$$

$$f_{rough} = \left[\frac{2}{3.2 \, \log_{10}(1/2 \, Re_b(f_{rough})^{1/2}) + 1.2} \right]^2$$

and

$$\phi_{ent} = 1 + \{(x/d)^{-0.7} * (T_w/T_b)^{0.1}\}$$

where x is the distance travelled along the tube, d is the hydraulic diameter of the tube, r is the hydraulic radius of the tube, R is the radius of curvature of the tube, x_{cv} is the distance along the tube from the beginning of the curved portion, L_{cv} is the total length of the curved portion of the tube, f_{rough} is the friction factor for a rough tube and f_{smooth} is the friction factor for a smooth tube. This correlation was used to match 95% of the available hydrogen data within ±20% (ref. 29). Supercritical methane experimental data has also been correlated with these equations (ref. 30). Because the equation takes property variations into account, it should predict Nusselt Numbers equally well for any supercritical Newtonian fluid, including carbon monoxide. Therefore, this heat transfer correlation is used in the carbon monoxide heat transfer analysis.

Oxygen Heat Transfer Correlations

The most general heat transfer equation for fully developed turbulent flow is

$$Nu = \frac{h * d}{k} = c(Re)^{a}(Pr)^{b} \tag{4.9}$$

where a, b, and c are determined experimentally for a given application. Spencer and Rousar (ref. 28) measured heat transfer to oxygen at supercritical pressure in electrically heated tubes. They combined their data with previous data to develop a heat transfer correlation for supercritical pressures and temperatures above 100 K (180 °R). An equation of the following form was assumed:

$$Nu = n * Re_f^{a} * Pr_f^{b} * \left(\frac{\mu_b}{\mu_w}\right)^{c} * \left(\frac{k_b}{k_w}\right)^{d} * \left(\frac{\rho_b}{\rho_w}\right)^{e} * \left(\frac{\hat{C}_{p-}}{C_p}\right)^{f}$$

$$\tag{4.10}$$

26 different correlations were developed before reaching one that matched

96% of the heat transfer measurements to within ± 30%. The following correlation was the best fit for the available experimental data:

$$Nu = .00243 \ Re_f * Pr_f^{.4} * \left(\frac{k_b}{k_w}\right)^{.530} * \left(\frac{\rho_b}{\rho_w}\right)^{-.486} * \left(\frac{\hat{C}_P}{C_P}\right)^{.638} * \left(\frac{P}{P_{cr}}\right)^{-.207}$$

(4.11)

This correlation was simplified by expressing the exponents as simple fractions

$$Nu = .0025 \ Re_f * Pr_f^{.4} * \left(\frac{k_b}{k_w}\right)^{1/2} * \left(\frac{\rho_b}{\rho_w}\right)^{-1/2} * \left(\frac{\hat{C}_P}{C_P}\right)^{2/3} * \left(\frac{P}{P_{cr}}\right)^{-1/5}$$

(4.12)

Even in its simplified version, this correlation still predicts over 95% of the test data within ±30%. This correlation is recommended by Spencer and Rousar (ref. 28) and has been used to accurately predict oxygen cooling conditions (ref. 32, 33, and 34). Equation (4.12) has been verified with experimental data over a pressure range of 17 to 34 MPa (2460 to 5000 psi) and for temperatures above 100 K (180 °R) for turbulent flow. The coolant pressure limitations of 46.0 MPa (6670 psi) for the maximum coolant inlet pressure and of 25.4 MPa (3690 psi) for the minimum coolant exit pressure would result in coolant pressures close to or in this range. Therefore, Equation (4.12) was selected for use in this analysis for liquid oxygen regenerative cooling.

CHAPTER V

THRUST CHAMBER CONTOUR OPTIMIZATION

Before the coolant channel geometry can be determined, the rocket thrust chamber contour should be optimized for the best engine performance. In order to optimize the thrust chamber contour, the engine requirements must be considered.

Thrust Chamber Performance Requirements

Three engines capable of delivering 445 kN (100,000 lbf) of thrust should be sufficient for the vehicle to reach an elliptical orbit for trans Earth injection (ref. 6). A chamber pressure of 22.1 MPa (3200 psi) is assumed to get maximum performance and a specific impulse of 245-320 seconds. Since the stoichiometric ratio for the $CO-O_2$ propellant combination is 0.571, a mixture ratio of 0.5 would allow for production of a small amount of oxygen for other uses when obtaining carbon monoxide and oxygen from carbon dioxide. The back pressure of the chamber should be above the Martian atmosphere pressure of 689 Pa (0.1 psi) to have fully developed flow in the rocket nozzle. Using these requirements as inputs to the CEC code (ref. 9), the characteristic exhaust velocity (C*), the combustion temperature, the thrust coefficient, and the specific impulse were determined for various exit area ratios. The exit area ratio is defined as the ratio of the exit area over the throat area.

Figure 15 shows the throat area of a combustion chamber with a short, conical nozzle. Table II shows the back pressure and specific impulse for various area ratios. To keep the back pressure above the ambient pressure, the area ratio must be less than 1400. As can be seen on Figure 16, a specific impulse gain is achieved up to 1400; however, increases in size and weight must considered as well as performance considerations. In a preliminary evaluation area ratios of 200, 600, and 1200 were compared to obtain a good cross-section of the most likely candidates for the descent/ascent vehicle.

Nozzle Contour Optimization

The Rao Method Optimum Nozzle Contour Program (ref. 10, 35) was used to optimize the thrust chamber nozzle for expansion area ratios of 200., 600, and 1200. This program can be used to calculate a supersonic exhaust nozzle contour for a given nozzle area ratio which gives maximum thrust for its length. The optimization method developed by Rao (ref. 35) uses the calculus of variations for an ideal gas, constant gamma expansion. The calculus of variations is used to establish geometric relationships that allow for calculations using the method of characteristics of an optimum nozzle contour. The required program inputs include the nozzle throat radius, the upstream and downstream radii of curvature normalized to the throat radius, combustion temperature, chamber pressure, molecular weight, ratio of specific heats, initial expansion angle, and the exit conditions (the expansion area ratio or the exit radius and length). Other inputs can be defaulted or are required only for certain options. For more details on the inputs, see ref. 10.

The nozzle throat radius was calculated from the CEC output and
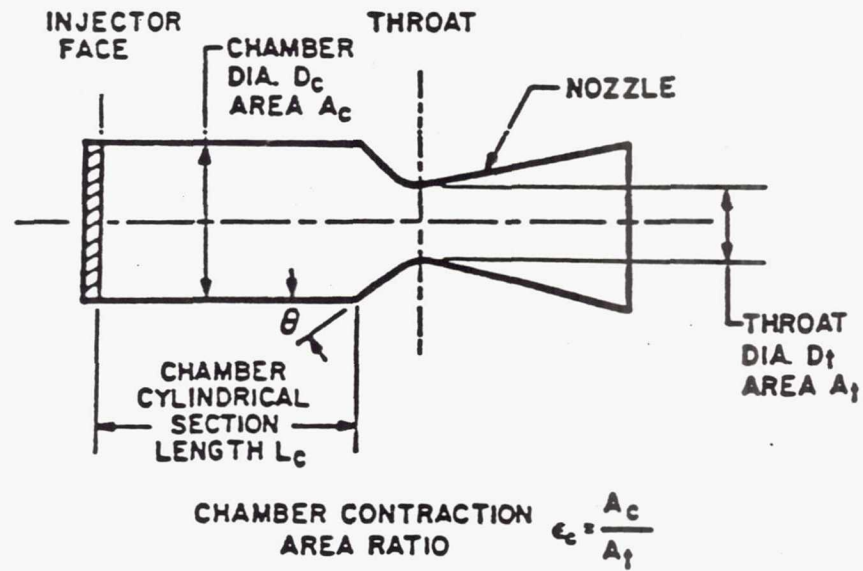
Figure 15.   Elements of Basic Cylindrical Combustion Chamber.
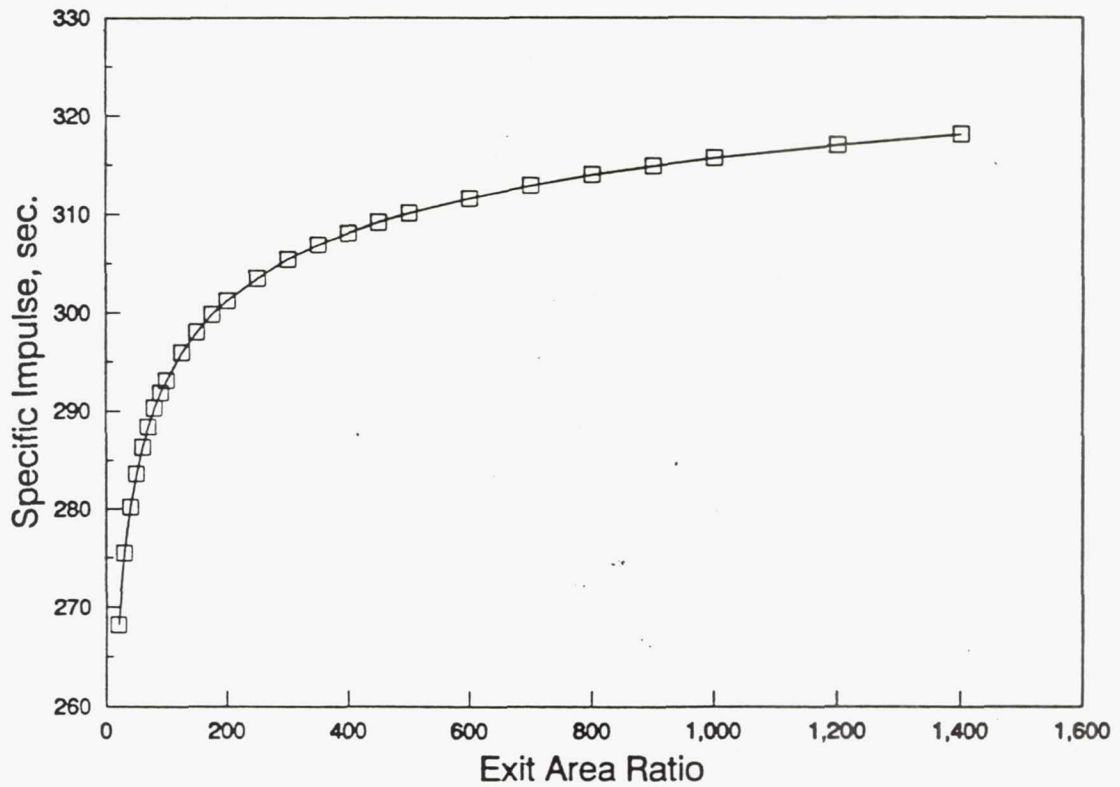
Figure 16.   Specific Impulse as a Function of Area Ratio for a Chamber
Pressure of 22.1 MPa and a Mixture Ratio of 0.50.

Table II.   Specific Impulse and Back Pressure for Various Exit Area
             Ratios at a Mixture Ratio of 0.50 and a Chamber Pressure
             of 22.1 MPa (3200 psi). (P_a = 689 Pa or 0.1 psi)

Exit Area Ratio	Vacuum Specific Impulse, sec	Back Pressure Pa	psi
20.0	268.2	147,000.	21.3
30.0	275.5	88,500.	12.8
40.0	280.2	61,750.	8.94
50.0	283.6	46,700.	6.76
60.0	286.3	37,200.	5.39
70.0	288.4	30,700.	4.45
80.0	290.3	26,000.	3.77
90.0	291.8	22,500.	3.25
100.0	293.1	19,700.	2.86
125.0	295.9	15,000.	2.17
150.0	298.0	11,950.	1.73
175.0	299.8	9,890.	1.43
200.0	301.2	8,390.	1.21
250.0	303.5	6,380.	0.924
300.0	305.4	5,100.	0.738
350.0	306.9	4,220.	0.611
400.0	308.1	3,580.	0.519
450.0	309.2	3,100.	0.449
500.0	310.1	2,730.	0.395
600.0	311.6	2,180.	0.316
700.0	312.9	1,810.	0.262
800.0	314.0	1,535.	0.222
900.0	314.9	1,330.	0.192
1000.0	315.7	1,168.	0.169
1200.0	317.0	935.	0.135
1400.0	318.1	774.	0.112
1600.0	319.0	658.	0.0952
1800.0	319.8	570.	0.0825
2000.0	320.5	500.	0.0725

thrust chamber requirements using the following rocket equations (ref. 11):

$$C_f = \frac{F}{A_t \, P_c} \qquad \text{or} \qquad A_t = \frac{F}{P_c \, C_f} \qquad (5.1)$$

where F is the thrust, P_c is the chamber pressure, C_f is the thrust coefficient, and A_t is the area of the throat. The throat area was calculated to be 91.93 cm^2 (14.25 in.^{2}) with a throat radius of 5.410 cm (2.130 in.).

The upstream and downstream radii of curvature of $1.0r_t$ and $0.4r_t$, respectively, were used, which are the "rule-of-thumb" values when designing combustion chambers. The combustion temperature, molecular weight, and ratio of specific heats were taken from the CEC code output (ref. 9).

The output from the Rao Method Optimum Nozzle Contour Program gives the nozzle mass flow and the corresponding nozzle contour. The output also includes the Mach number, specific impulse, gas pressure, gas density, and gas temperature for each axial location. Table III gives the coordinates for the optimized nozzles for expansion area ratios of 200., 600., and 1200.

Combustion Chamber Geometry

The combustion chamber geometry is determined using equations from the ref. 11. The throat area is generally the starting point in designing the combustion chamber. A cylindrical combustion chamber is assumed, which is used most frequently in the U.S. and is less difficult to manufacture than other possible shapes. For most turbopump-fed, high thrust, and high pressure engine systems, a low chamber contraction ratio is used, generally 1.3 to 3.0. To keep the combustion chamber as short as possible, a high contraction ratio is used, thereby reducing the

Table III. Coordinates for RAO Optimized Nozzle Contour for Expansion
Ratios of 200., 600., and 1200.

ϵ = 200.		ϵ = 600.		ϵ = 1200.	
Radius	Nozzle Length	Radius	Nozzle Length	Radius	Nozzle Length
cm	cm	cm	cm	cm	cm
5.587	0.0	5.469	0.0	5.410	0.0
6.098	1.422	5.959	1.380	5.950	1.43
6.288	1.651	6.648	2.211	6.633	2.192
6.755	2.205	7.792	3.542	7.528	3.162
7.886	3.518	9.279	5.238	9.479	5.229
9.328	5.177	11.253	7.493	12.278	8.202
11.197	7.353	13.92	10.619	16.40	12.75
13.544	10.258	19.53	17.66	21.99	33.96
16.285	14.043	31.01	34.52	50.09	62.45
19.336	18.514	41.53	53.13	70.82	105.16
26.932	30.682	54.19	79.93	93.68	164.7
35.119	46.225	64.10	104.7	107.17	207.2
44.411	67.772	79.54	151.2	125.7	276.5
53.944	95.366	92.41	199.2	145.7	371.1
62.951	128.46	107.48	270.8	167.9	512.4
71.898	171.82	121.99	364.8	182.5	643.1
79.011	219.45	133.95	479.7	187.4	702.3

chamber length for a given volume. A contraction ratio of 2.96 was assumed, which is the contraction ratio of the Space Shuttle Main Engine. To calculate the combustion chamber length for a cylindrical combustion chamber, the equation was used for a approximate value of the combustion chamber volume, which is typically defined as the space from the injector face to the nozzle throat plane (Figure 15),

$$Vol_c = A_t \left(L_c * \epsilon_c + .333 r_t \cot\theta_c (\epsilon_c^{.333} - 1) \right) \tag{5.6}$$

where ϵ_c is the chamber contraction area ratio, θ_c is the chamber contraction angle (typically 30°), A_t is the throat area, and L_c is the length of the combustion chamber. The theoretical required chamber volume is proportional to the mass flow rate of the propellants, m_{tc}, the average specific volume, v, and the stay time necessary for efficient combustion, t_s, (ref. 11):

$$Vol_c = m_{tc} * v * t_s \tag{5.7}$$

The m_{tc} and v are calculated in the Rao Optimization Program, but the stay time must be determined empirically for a given propellant combination. Propellant stay times of .002 - .04 seconds have been used in various combustion chamber designs (ref. 11). Substituting equation (5.7) into (5.6) and solving for the chamber length, L_c, gives

$$L_c = \frac{1}{\epsilon_c} \left(\frac{m_{tc} \, v \, t_s}{A_t} - .333 r_t \cot\theta_c (\epsilon_c^{.333} - 1) \right) \tag{5.8}$$

The only unknown is t_s, which was assumed to be .004 sec so that the chamber would not be too large and bulky. The L_c was calculated to be 76.2 cm (30.00 in.). The contour of the chamber from the throat to the cylindrical section of the chamber was calculated using geometry relations and an upstream throat radius of curvature of $1.0 r_t$.

The final thrust chamber contours are shown in Figures 17, 18, and
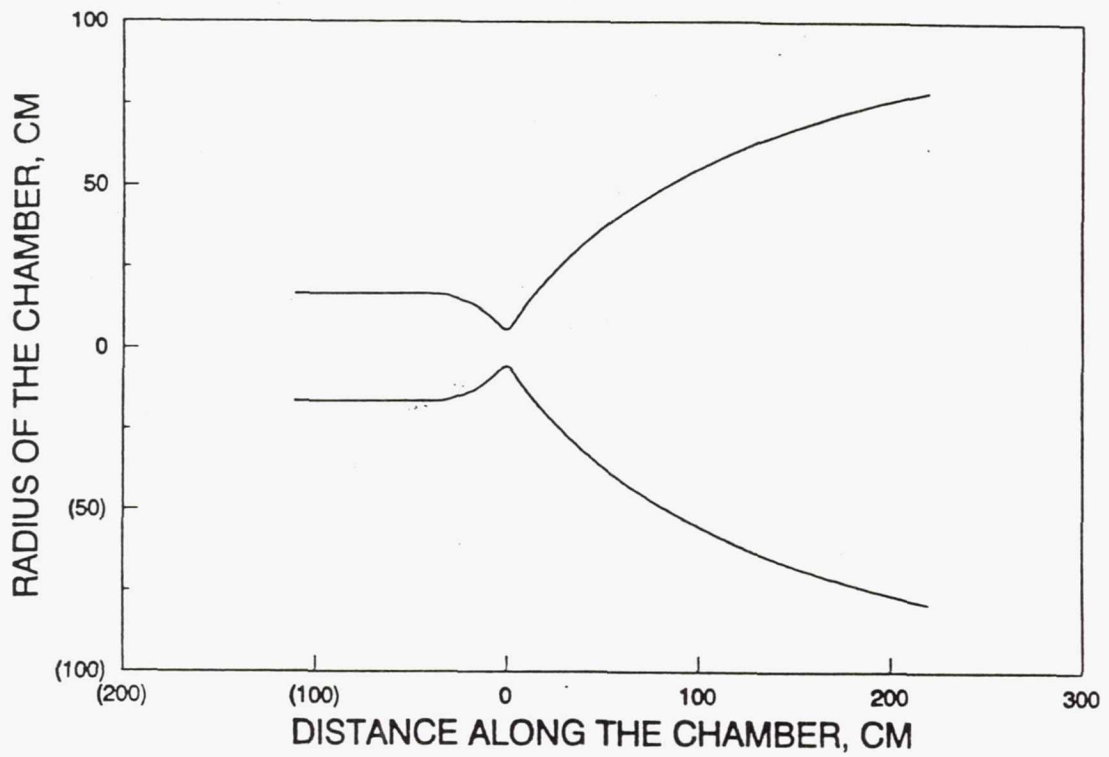
Figure 17. Optimized Thrust Chamber Contour for an Expansion Ratio
of 200.
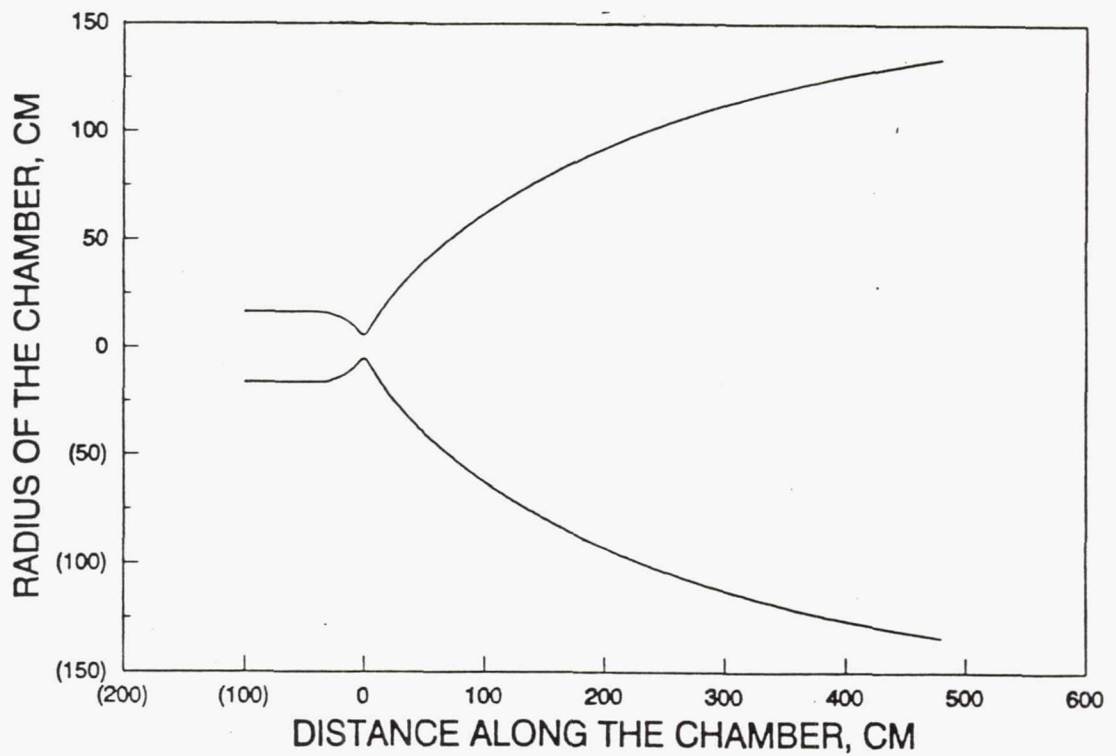
Figure 18. Optimized Thrust Chamber Contour for an Expansion Ratio
of 600.

19. The added size and weight were not significant relative to the increased specific impulse of an exit area ratio for 1200 over an exit ratio of 200 and 600. Therefore, the highest exit area ratio is selected for use. The radial and axial values for various points on the contour are given in Table IV.
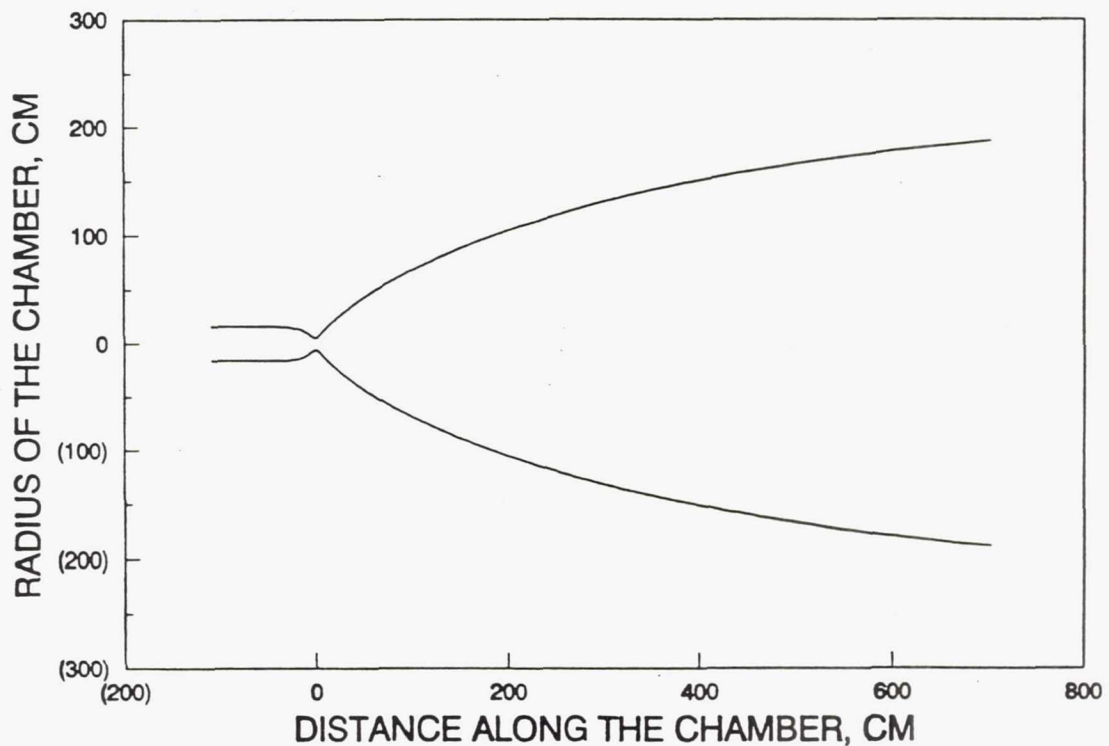
Figure 19. Optimized Thrust Chamber Contour for an Expansion Ratio of 1200.

Table IV.   Radial and Axial Values for the Optimized Chamber Contour
             (x=0 is the Throat. Negative Axial Locations are Upstream
             of the Throat and Positive Axial Locations are Downstream
             of the Throat.)

Axial Location		Radius	
cm	in.	cm	in.
-109.6	-43.17	16.01	6.304
-96.94	-38.17	16.01	6.304
-84.24	-33.17	16.01	6.304
-71.54	-28.17	16.01	6.304
-58.84	-23.17	16.01	6.304
-46.14	-18.17	16.01	6.304
-33.44	-13.17	16.01	6.304
-29.27	-11.52	15.65	6.160
-25.23	-9.931	14.56	5.734
-13.96	-5.498	13.96	5.498
-2.705	-1.065	6.134	2.415
-1.400	-0.551	5.594	2.202
0.000	0.000	5.410	2.130
1.430	0.563	5.950	2.342
2.192	0.863	6.633	2.611
3.162	1.245	7.528	2.964
5.229	2.059	9.479	3.732
8.202	3.229	12.278	4.834
12.75	5.020	16.40	6.457
33.96	13.37	21.99	8.657
62.45	24.59	50.09	19.72
105.16	41.40	70.82	27.88
164.7	64.84	93.68	36.88
207.2	81.57	107.17	42.19
276.5	108.8	125.7	49.49
371.1	146.1	145.7	57.36
512.4	201.7	167.9	66.10
643.1	253.2	182.5	71.85
702.3	276.5	187.4	73.78

CHAPTER VI

ROCKET ENGINE HEAT TRANSFER EVALUATION PROGRAM

A rocket engine heat transfer evaluation program (REHTEP) was used to evaluate the thrust chamber heat transfer characteristics. The code predicts heat flux through a thrust chamber wall, assuming one-dimensional conduction and convection at up to 25 axial locations along the chamber length. Figure 20 shows a schematic of a typical thrust chamber with a cutaway at one axial location. This code has been used extensively to predict results for in-house programs at the Lewis Research Center. The code utilizes the Complex Chemical Equilibrium Composition computer program (ref. 9) for the hot-gas side calculations and the FLUID program (ref. 12) to obtain coolant properties. The inputs to the REHTEP include the composition of the fuel/oxidant mixture, the propellant and coolant flow rates, chamber pressure, coolant entrance temperature and pressure, the chamber geometry, the type of chamber material, and the fluid heat transfer correlation coefficients at the coolant wall and the hot-gas wall. Outputs of temperature, enthalpy, conductivity, density, viscosity, specific heat, and Prandtl and Reynolds numbers are given on the hot-gas side of the chamber (reference conditions only) and in the coolant channels (static, stagnation, reference, wall, and/or film conditions). The friction pressure loss and

39
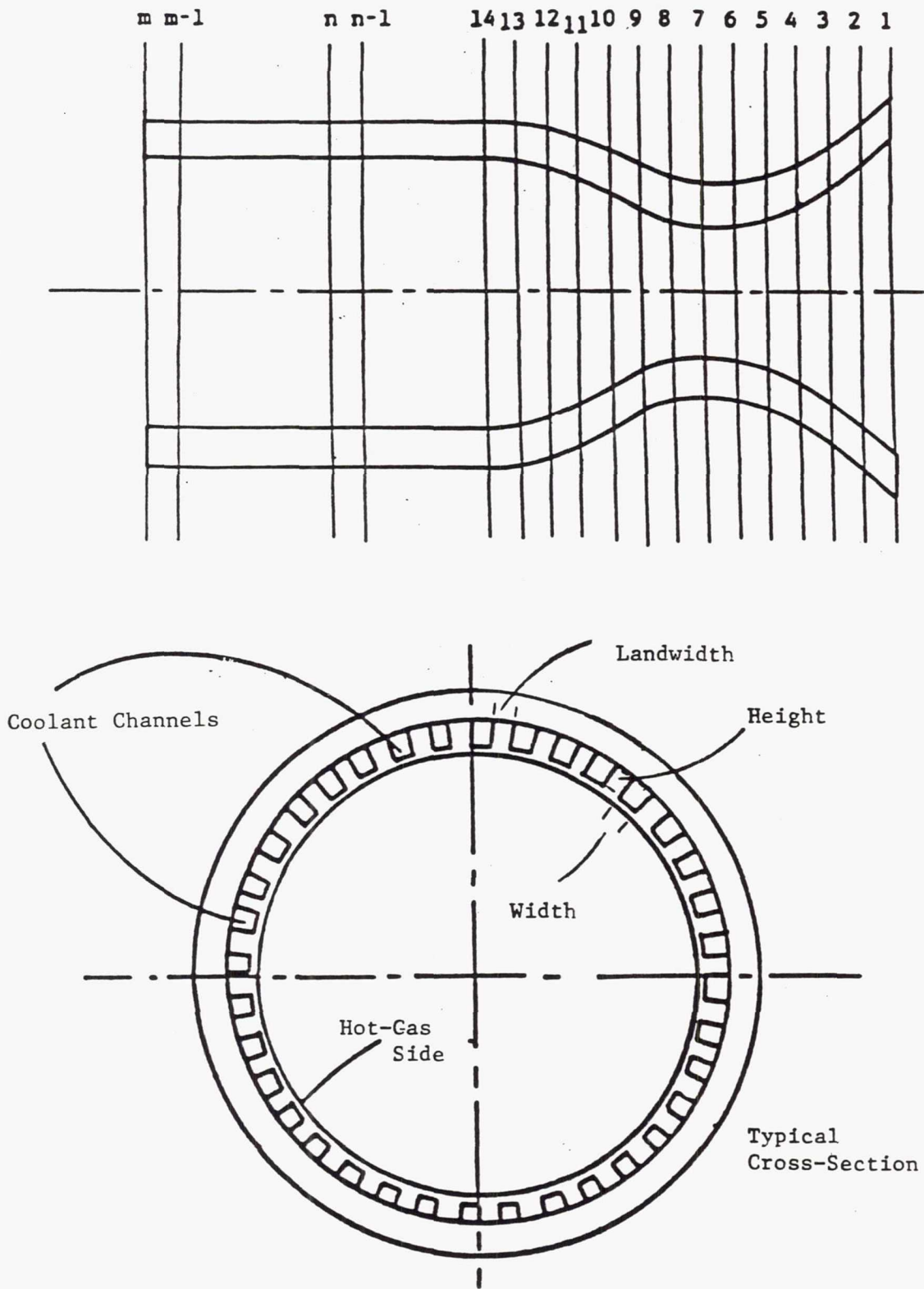
Figure 20. Schematic of Typical Thrust Chamber with a Cutaway Showing the Coolant Channels.

momentum pressure loss in the coolant channels are also calculated for output, along with the heat transfer coefficients and heat fluxes for the coolant side and the hot-gas side. The friction pressure loss equation is

$$f.p.l. = f * \tfrac{1}{2}(\rho_b(n-1) + \rho_b(n)) * \tfrac{1}{2}(V(n-1) + V(n))^2 *$$

$$\frac{x(n)-x(n-1)}{g_c * \tfrac{1}{2}(d_c(n-1) + d_c(n))} \qquad (6.1)$$

where

$$f = 4(.004 + \frac{.125}{(Re_b)^{.32}})$$

and n is the location at which calculation are being made and n-1 is the previous location. The momentum pressure loss equation is

$$m.p.l. = \frac{m_{c}^2}{g_c} \left[\frac{1}{\tfrac{1}{2}(A_c(n-1)*N_c(n-1) + A_c(n)*N_c(n))} \right] *$$

$$\left[\frac{1}{\rho_b(n)*A_c(n)*N_c(n)} - \frac{1}{\rho_b(n-1)*A_c(n-1)*N_c(n-1)} \right] \qquad (6.2)$$

In a recent experimental program at the Lewis Research Center, REHTEP was used to predict wall temperatures and pressure drops for a copper combustion chamber. The computer results were then compared with the experimental results. Figure 21 shows the combustion chamber during a hot firing in the Rocket Engine Test Facility, Stand A. The purpose of the testing was to evaluate the ability of liquid oxygen to cool a hydrocarbon-fueled combustion chamber. The chamber was cooled with liquid oxygen using kerosene and liquid oxygen as propellants. A comparison is shown in Figure 22 between experimental thermocouple data from this chamber tested at a mixture ratio of 2.2 and a chamber pressure of 8.89 MPa (1290 psia) and the computer results using the REHTEP. Sets of four thermocouples were located at five axial locations, as indicated on the graph. The four thermocouples were 90 degrees apart

42
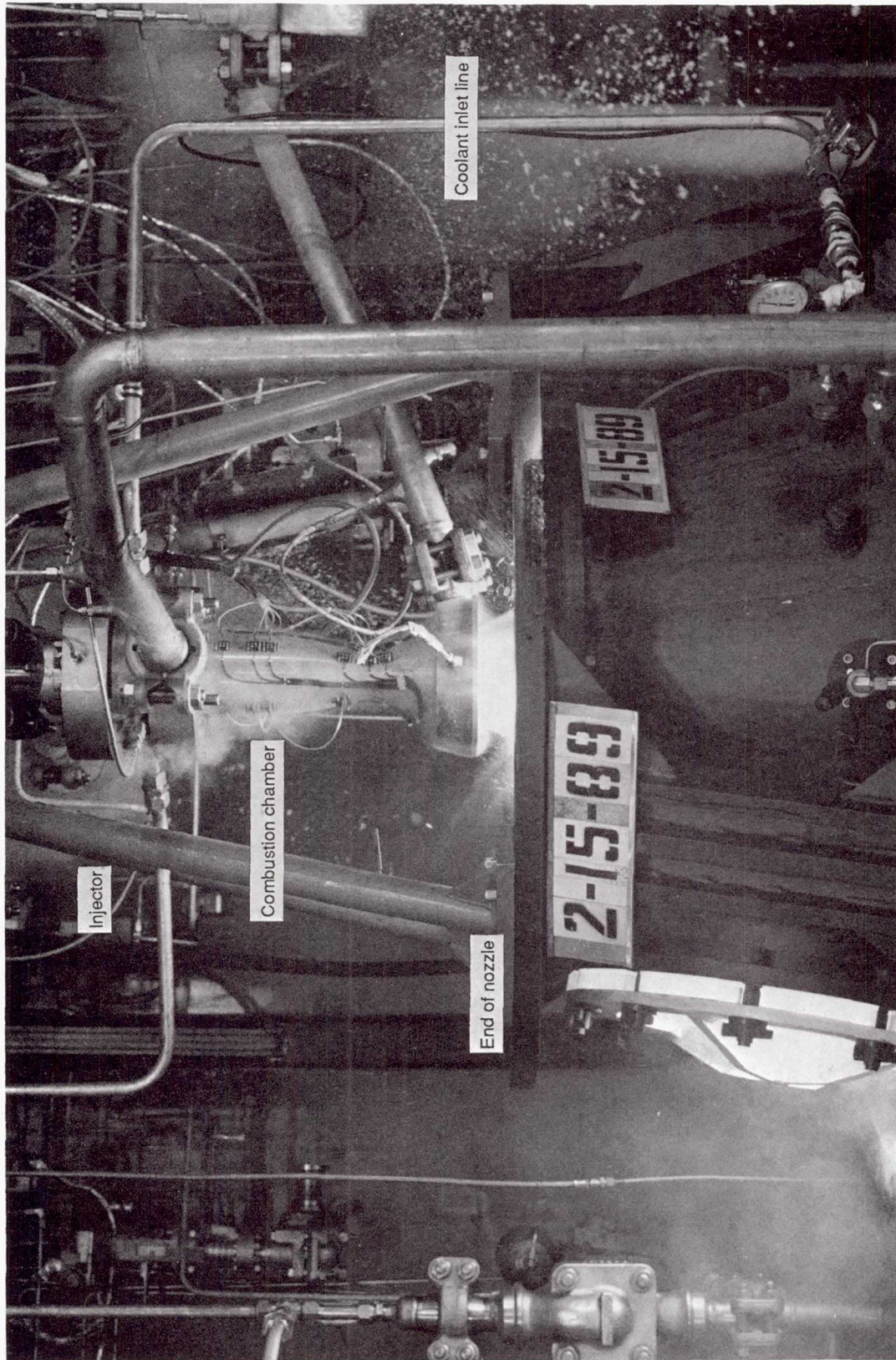
Figure 21. Liquid-Oxygen-Cooled Combustion Chamber During Hot-Firing
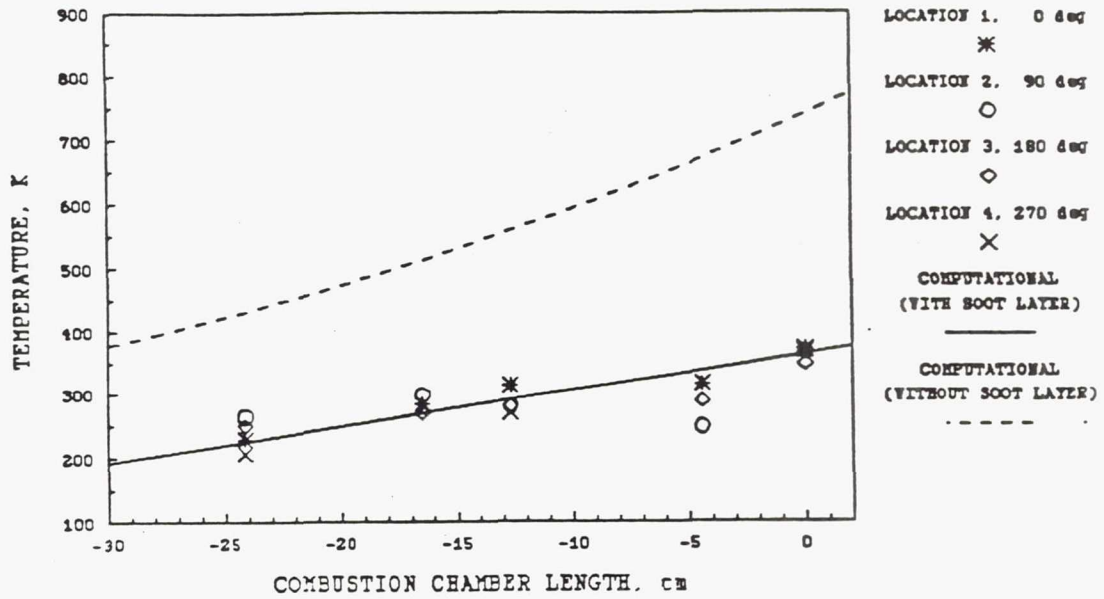
Figure 22.   Comparison of Computational and Experimental Data for a
Mixture Ratio of 2.2 and a Chamber Pressure of 8.89 MPa.
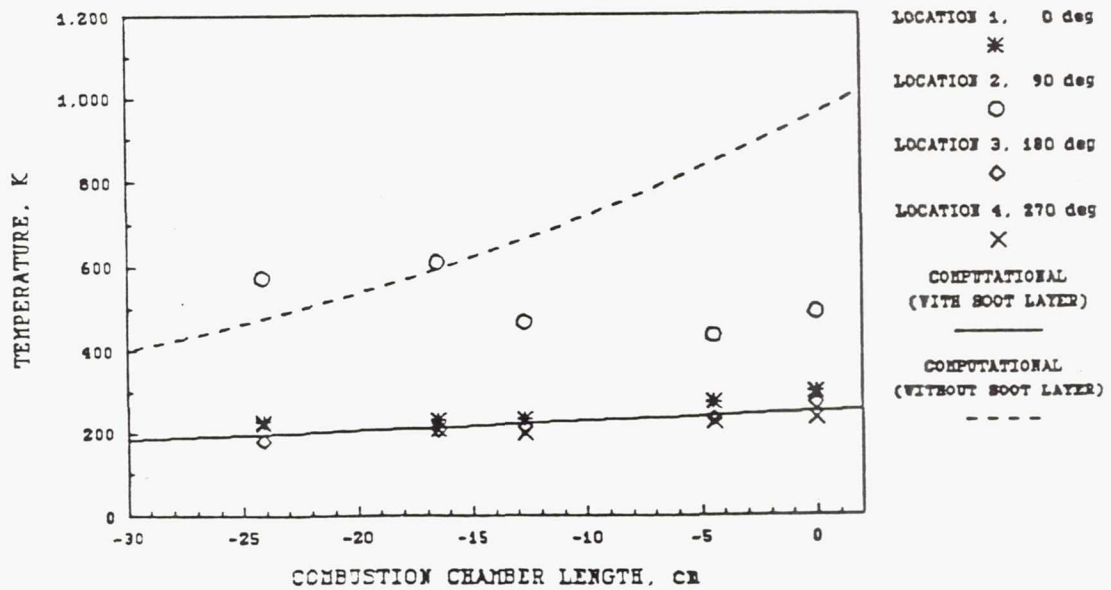
Figure 23.   Comparison of Computational and Experimental Data for a
Mixture Ratio of 1.8 and a Chamber Pressure of 8.48 MPa.

circumferentially.

The throat position is at 0.00 cm and the negative chamber lengths indicate that the temperature readings are upstream of the chamber throat. The upper line represents the evaluation program results with no soot layer on the chamber wall. The lower line represents the results if a .025 mm (.001 in.) soot layer has been deposited on the chamber wall. When combusting kerosene and oxygen propellants, soot particles precipitate from the combustion gases and adhere to the chamber wall, forming a coating. The Systems Improved Numerical Differencing Analyzer (SINDA) program (ref. 36) was used to predict the soot level in the chamber for the given chamber pressure and mixture ratio, based on previous experimental soot measurements during test firings. As can be seen, the evaluation program prediction with soot is within the data scatter.

A comparison is shown in Figure 23 between the REHTEP results and thermocouple data from the same chamber when tested at a mixture ratio of 1.8 and a chamber pressure of 8.48 MPa (1230 psia). The SINDA program predicted a .051 mm (.002 in.) soot layer on the chamber wall under these operating conditions. The evaluation program results using this soot layer are represented by the lower line. The upper line represents the code prediction without soot. Again the code prediction is within the data scatter, except for location 2. Upon inspection of the data and the chamber, the soot layer at this location did not seem to be as thick as at the other locations, and there was no soot layer close to the injector.

As can be seen, the evaluation program has predicted hot-gas-side wall temperatures for combustion of kerosene and liquid oxygen. It has

also been used to predict hot-gas-side wall temperatures for combustion of gaseous hydrogen and liquid oxygen. From these data, it can be extrapolated that the code can predict the hot-gas-side wall temperatures for combustion of carbon monoxide and oxygen, as is done in the next chapter.

CHAPTER VII

COOLANT CHANNEL GEOMETRY OPTIMIZATION

To optimize the coolant channel geometry, the REHTEP (Rocket Engine Heat Transfer Evaluation Program) is used to determine coolant pressure drop and hot-gas-side wall temperature. The optimum coolant channel configuration is defined as that which gives the lowest pressure drop for a given hot-gas-side wall temperature. The possible configurations are limited by structural, mechanical, and material constraints. Therefore, not every conceivable configuration is evaluated, but only those within these constraints.

Due to the limitations of present-day turbomachinery, the maximum coolant inlet pressure for the thrust chamber is 42.0 MPa (6090 psia). The minimum coolant exit pressure is 25.4 MPa (3685 psia) for a chamber pressure of 22.0 MPa (3200 psia), assuming a 15% pressure drop across the injector face, which is necessary for combustion stability. These constraints limit the coolant pressure drop to 16.6 MPa (2390 psia).

To increase the extraction of heat from the combustion gases, the combustion chamber liner is built from a high-conductivity material such as copper or a copper alloy. Also, the combustion chamber wall should be operated in the material's elastic region to avoid plastic deformation which might limit the chamber's life. To keep a copper or copper-alloy

chamber in its elastic region, the hot-gas-side wall temperature should be kept below 778 K (1400 R). The lower the temperature is, the less likely deformation of the chamber wall will occur.

As the combustion gases expand through the nozzle of the chamber, they become cooler and have less heat to be extracted by the coolant. At some axial location along the chamber, the wall temperature of the chamber wall material can be kept below its melting point without a coolant, using only radiation cooling. For the chosen chamber geometry, this axial location was 19.41 cm (7.64 in.) from the throat at an area ratio of 16.57. Therefore, no coolant is necessary beyond this point and for coolant purposes, the chamber is assumed to be only 19.41 cm (7.64 in.) in length.

To withstand the thermal and pressure loads on the combustion chamber wall, the distance between the coolant channels should be roughly equal to the coolant channel width. Figure 20 shows a schematic of the cross-section of several coolant channels with the width, height, and landwidth (distance between coolant channels) labelled. If the landwidth is much thinner than the channel width, the chamber wall will not be properly supported and will not withstand the pressure loads. If the fin is much wider than the channel width, the thermal gradient in the wall will be large, resulting in deformation.

The height-to-width ratio, or aspect ratio, of the coolant channel should be kept below eight. The purpose of having a high aspect ratio is to increase the surface area of the passages for a given cross-sectional area. The heat transfer area between the wall and the coolant is thereby increased. This increased heat transfer phenomenon starts to level out around an aspect ratio of six. Therefore, a practical limit

would be an aspect ratio of eight, after which the increased heat transfer phenomenon plateaus.

For optimum cooling, the number of cooling channels might vary as the area ratio of the combustion chamber decreases and increases. However, frequent variations are impractical and often impossible when considering actual manufacture. Because of the manufacturing limitations, the total number of cooling channels should only increase or decrease by factors of integers (i.e. the change in the number of cooling passages would be a factor of 2, 3, 4, etc.). Figure 24 shows how the number of cooling channels can change. Also, many variations would result in higher manufacturing costs than a few variations would.
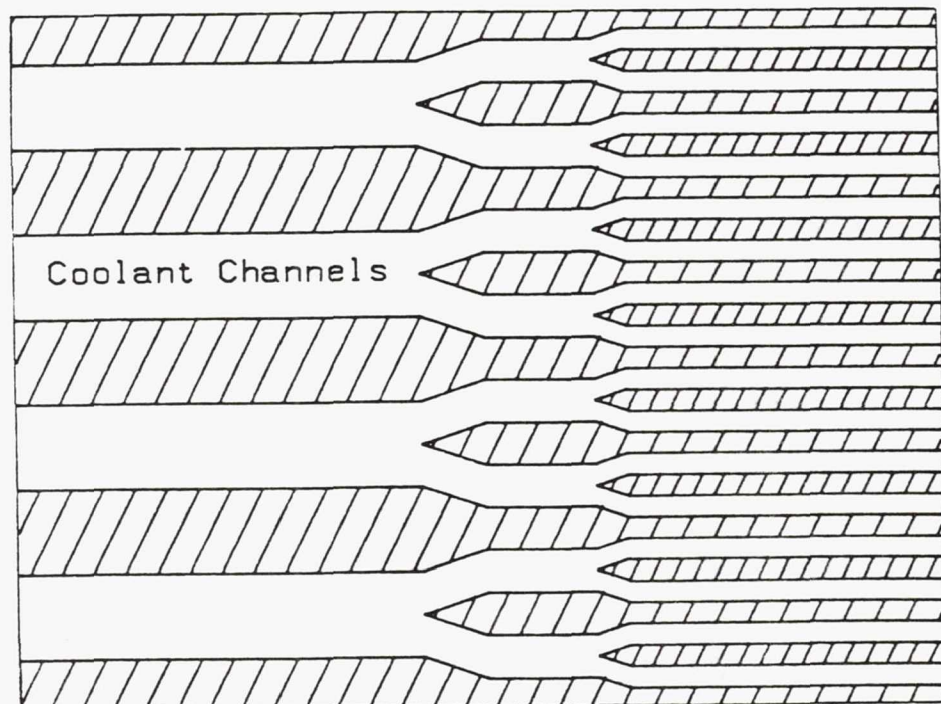
Figure 24. Schematic of Bifurcation of Coolant Channels.

With these limitations in mind, the coolant channel geometry is optimized separately for oxygen cooling and carbon monoxide cooling. The method used for optimization and the results of this method are given below.

Oxygen Cooling Geometry

A base configuration was established from data for other chambers (ref. 32 - 34) and the base configuration is given in Table V. From this base, the coolant flowrate, coolant channel aspect ratio (height-to-width ratio), and the coolant channel width were parametrically varied. The amount of coolant was constrained by the amount of oxygen available. At a mixture ratio (oxygen-to-fuel) of 0.500 and a total mass flowrate (as calculated from the Rao Method of Optimization) of 152.9 kg/sec (337.1 lbm/sec), only 50.97 kg/sec (112.4 lbm/sec) is available for regenerative cooling. Each geometry configuration was analyzed at four flowrates initially to determine the trend for the given configuration. The flowrates were 27.21 kg/sec (60.00 lbm/sec), 36.29 kg/sec (80.00 lbm/sec), 45.36 kg/sec (100.0 lbm/sec), and 50.97 kg.sec (112.4 lbm/sec).

In the analysis, the width was kept constant as the aspect ratio was varied from one to eight (Table VI). However, the results for an aspect ratio of 1 and a flowrate of 50.97 kg/sec (112.4 lbm/sec) had such a high wall temperature and high pressure, that this geometry was not evaluated further. The results for the other aspect ratios show that the pressure drop decreased significantly with increasing aspect ratio (Figure 25), but the temperature rose above the material limitations. The dotted lines on the figure represent the temperature and pressure drop limitations. The width was halved as the aspect ratio was varied from 4 to 8 (Table VI). The pressure drop was larger than 16.6 MPa (2390

Table V. Base Configuration Chamber Geometry for Oxygen and Carbon
Monoxide Cooling (Aspect Ratio of One)

Distance	Contour Diameter	Cooling Channel Width	Cooling Channel Height	Cooling Channel Area	Number of Cooling Channels
cm	cm	cm	cm	cm^2	
-109.6	32.02	0.1473	0.1473	0.02170	350
-96.94	32.02	0.1473	0.1473	0.02170	350
-84.24	32.02	0.1473	0.1473	0.02170	350
-71.54	32.02	0.1473	0.1473	0.02170	350
-58.84	32.02	0.1473	0.1473	0.02170	350
-46.14	32.02	0.1473	0.1473	0.02170	350
-33.44	32.02	0.1473	0.1473	0.02170	350
-29.27	31.30	0.1422	0.1422	0.02023	350
-25.23	29.12	0.1321	0.1321	0.01744	350
-13.96	27.92	0.1270	0.1270	0.01613	350
-2.705	12.27	0.1118	0.1118	0.01249	175
-1.400	11.19	0.1016	0.1016	0.01032	175
0.000	10.82	0.09906	0.09906	0.009813	175
1.430	11.90	0.1067	0.1067	0.01138	175
1.632	12.26	0.1092	0.1092	0.01193	175
1.904	12.74	0.1168	0.1168	0.01365	175
3.162	15.06	0.1372	0.1372	0.01881	175
3.910	16.46	0.1473	0.1473	0.02170	175
5.734	19.91	0.1778	0.1778	0.03161	175
6.868	22.06	0.09906	0.09906	0.009813	350
8.202	24.56	0.1092	0.1092	0.01193	350
9.787	27.48	0.1219	0.1219	0.01486	350
13.92	34.83	0.1549	0.1549	0.02401	350
16.54	39.27	0.1727	0.1727	0.02983	350
19.41	43.98	0.1905	0.1905	0.03629	350

Table VI.   Cooling Channel Geometries at the Throat Location for all
            Preliminary Configurations.

Aspect Ratio	Cooling Channel Width cm	Cooling Channel Height cm	Cooling Channel Area cm^2	Number of Cooling Channels
1.	0.0990	0.0990	0.00980	175
2	0.0990	0.198	0.0196	175
3	0.0990	0.297	0.0294	175
4	0.0990	0.396	0.0392	175
5	0.0990	0.495	0.0490	175
6	0.0990	0.594	0.0588	175
7	0.0990	0.693	0.0686	175
8	0.0990	0.792	0.0784	175
4	0.0495	0.198	0.00980	350
5	0.0495	0.247	0.0122	350
6	0.0495	0.297	0.0147	350
7	0.0495	0.346	0.0172	350
8	0.0495	0.396	0.0196	350
6	0.0330	0.198	0.00653	520
7	0.0330	0.231	0.00762	520
8	0.0330	0.264	0.00871	520
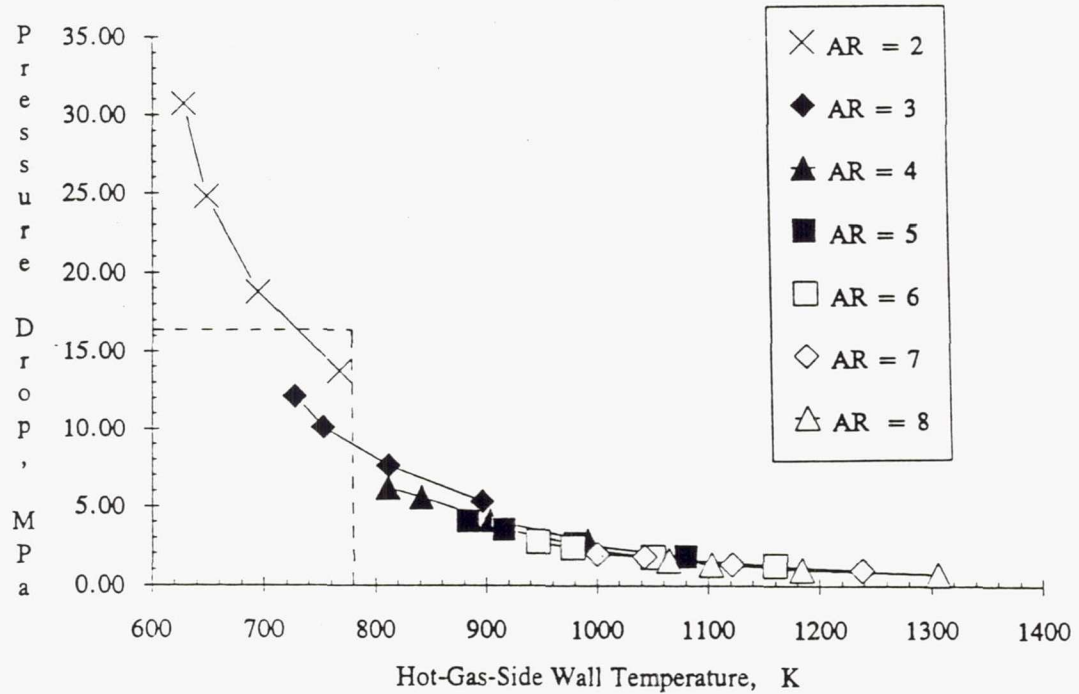
Figure 25. Pressure Drop and Wall Temperature Values for Aspect Ratios from 2 to 8 at the Baseline Width (Oxygen Cooling).

psia) for aspect ratios lower than four. The results again show a decrease in pressure drop with increasing aspect ratio. However, now the temperatures stayed in range, giving the lowest pressure drop for a given hot-gas-side wall temperature at an aspect ratio of eight (Figure 26).

The width was reduced again to a third of the baseline width, w_{bl}, while the aspect ratio was varied from six to eight (Table VI). Again, the pressure was greater than 16.6 MPa (2390 psia) for aspect ratios lower than six. None of these configurations were within the pressure and temperature constraints (Figure 27). Because the coolant pressure drop was so large at this width, thinner widths were not considered.
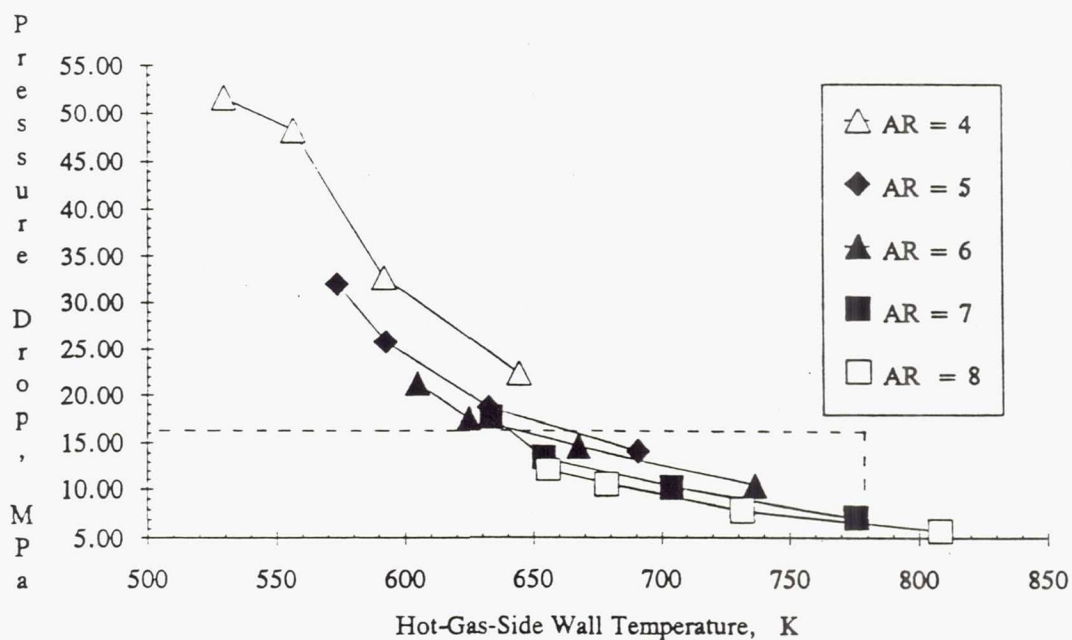
Figure 26. Pressure Drop and Wall Temperature Values for Aspect Ratios from 4 to 8 at Half the Baseline Width (Oxygen Cooling).
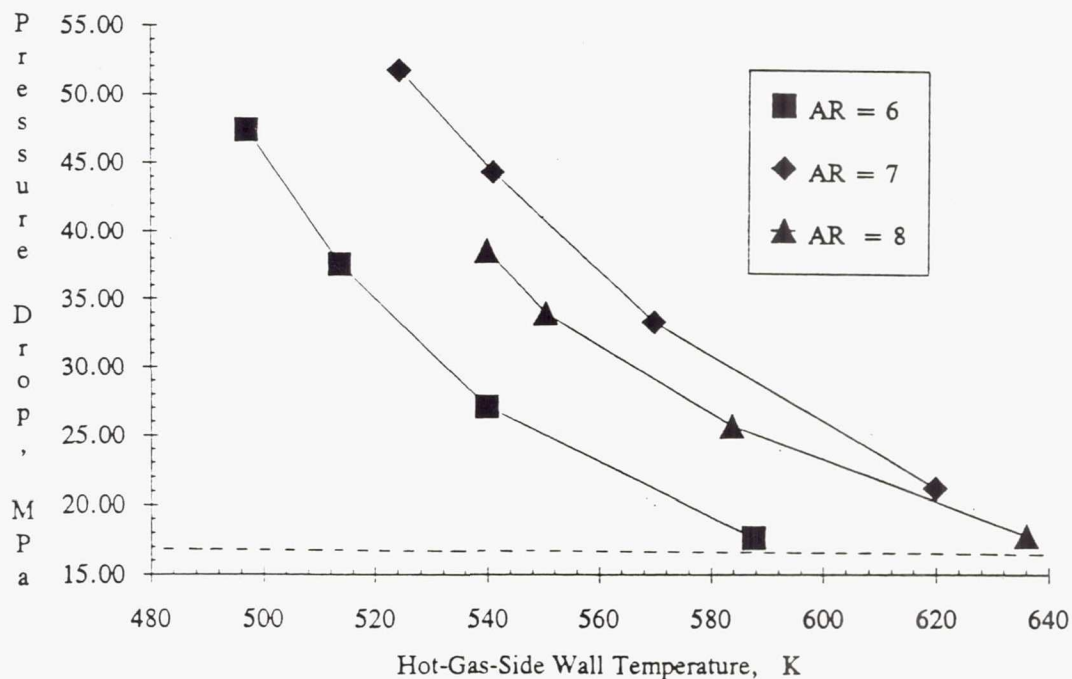
Figure 27. Pressure Drop and Wall Temperature Values for Aspect Ratios from 6 to 8 at One Third the Baseline Width (Oxygen Cooling).

After determining a range where the optimum geometry is likely to be, the coolant channel width was varied between .45w_{bl}, and .65w_{bl} at an aspect ratio of 8. An aspect ratio of 7.5 was also tried, but did not give as low a pressure for a given temperature as an aspect ratio of 8. These configurations are shown in Figure 28. An aspect ratio of 8 with a width of .6w_{bl} gives the lowest pressure drop for a given wall temperature. At the highest possible flow, the temperature is 744 K (1339 R), which is very close to the maximum allowable temperature. Therefore, a width of .55w_{bl} was chosen because it has the second lowest pressure drop for a given hot-gas-side wall temperature while the temperature is 702 K (1264 R) at a flowrate of 50.97 kg/sec (112.4 lbm/sec).
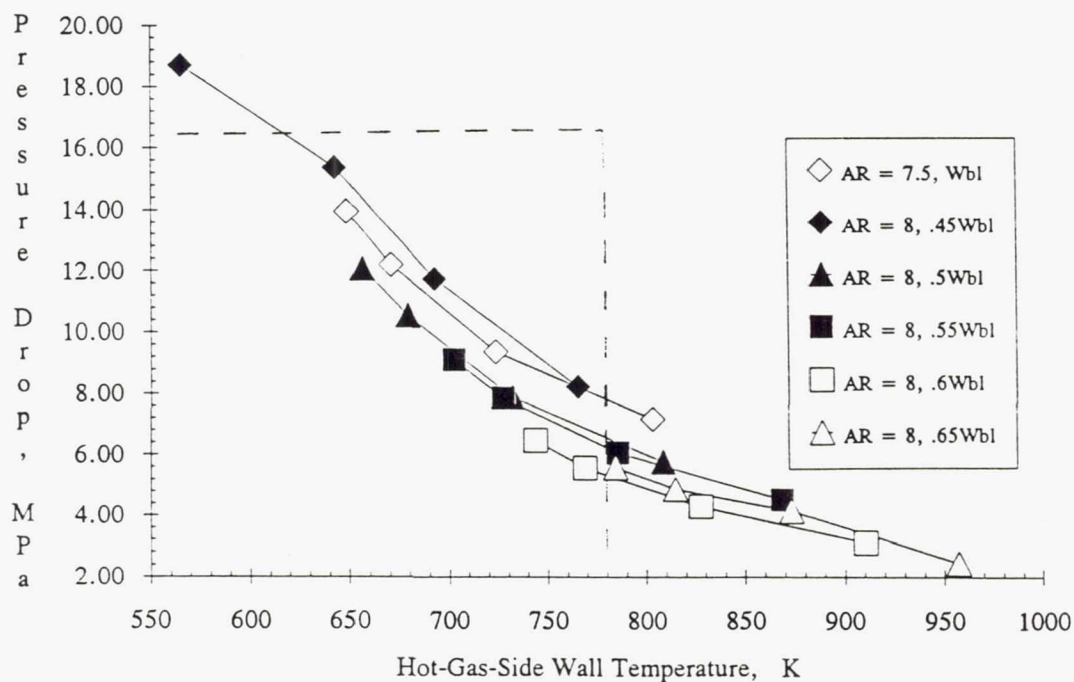
Figure 28. Pressure Drop and Wall Temperature Values for Aspect Ratios of 7.5 and 8 at Various Widths (Oxygen Cooling).

Carbon Monoxide Geometry

The carbon monoxide analysis used the same base configuration as the oxygen analysis, as given in Table V. The amount of coolant was constrained by the amount of carbon monoxide available. At a mixture ratio (oxygen-to-fuel) of 0.500 and a total mass flowrate (as calculated from the Rao Method of Optimization) of 152.9 kg/sec (337.1 lbm/sec), 101.9 kg/sec (224.7 lbm/sec) is available for regenerative cooling. Each geometry configuration was analyzed at ten flowrates initially to determine the trend for the given configuration. Four of the flowrates were 27.21 kg/sec (60.00 lbm/sec), 36.29 kg/sec (80.00 lbm/sec), 45.36 kg/sec (100.00 lbm/sec), and 50.97 kg.sec (112.40 lbm/sec). These were chosen to match the flowrates for the oxygen cooling. The other six flowrates were 54.43 kg/sec (120.00 lbm/sec), 63.50 kg/sec (140.0 lbm/sec), 72.57 kg/sec (160.00 lbm/sec), 81.65 kg/sec (180.0 lbm/sec), 90.72 kg/sec (200.0 lbm/sec), and 101.9 kg/sec (224.7 lbm/sec). If the pressure drop reached 50.0 MPa (7250 psia) at any of these flowrates, no higher flowrates were evaluated for that configuration.

In the preliminary analysis, the width was kept constant as the aspect ratio was varied from one to eight (Table VI). The results show that the pressure drop decreased significantly with increasing aspect ratio (Figure 29). An aspect ratio of eight gives the lowest pressure drop of these configurations for a given hot-gas-side wall temperature.

The width was halved as the aspect ratio was varied from 6 to 8 (Table VI). The pressure drop was larger than 16.6 MPa (2390 psi) for aspect ratios lower than six. The results again show a decrease in pressure drop with increasing aspect ratio. None of these configurations were an improvement over the baseline-width results. The width was
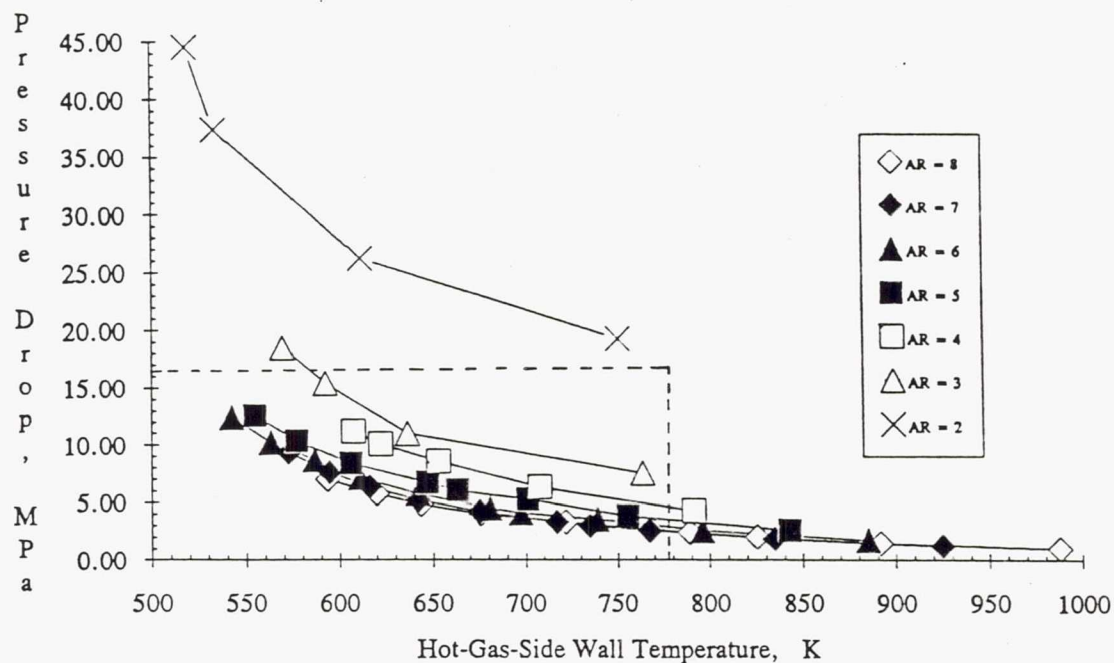
Figure 29.   Pressure Drop and Wall Temperature Values for Aspect
Ratios from 2 to 8 at the Baseline Width (Carbon Monoxide
Cooling).

reduced again to $1/3w_{bl}$ while the aspect ratio was varied from six to
eight.   The pressure was greater than 16.6 MPa (2390 psia) for all of
these aspect ratios, as shown in Figure 30.   Therefore, no further
reduction in width was considered.

After determining a range where the optimum geometry is likely to
be, aspect ratios in that range were evaluated at the baseline width.
Aspect ratios of 7.25, 7.5, and 7.75 were compared with aspect ratios of
7.0 and 8.0.   These configurations are shown in Figure 31.   Although an
aspect ratio of 7.5 seemed to be best, the results at 8.0 were very
close.   Hence, the channel widths of .75 and 1.5 w_{bl} were tried.

As the width was expanded or contracted from the baseline width,
the pressure drop increased for a given wall temperature.   Widths of .9
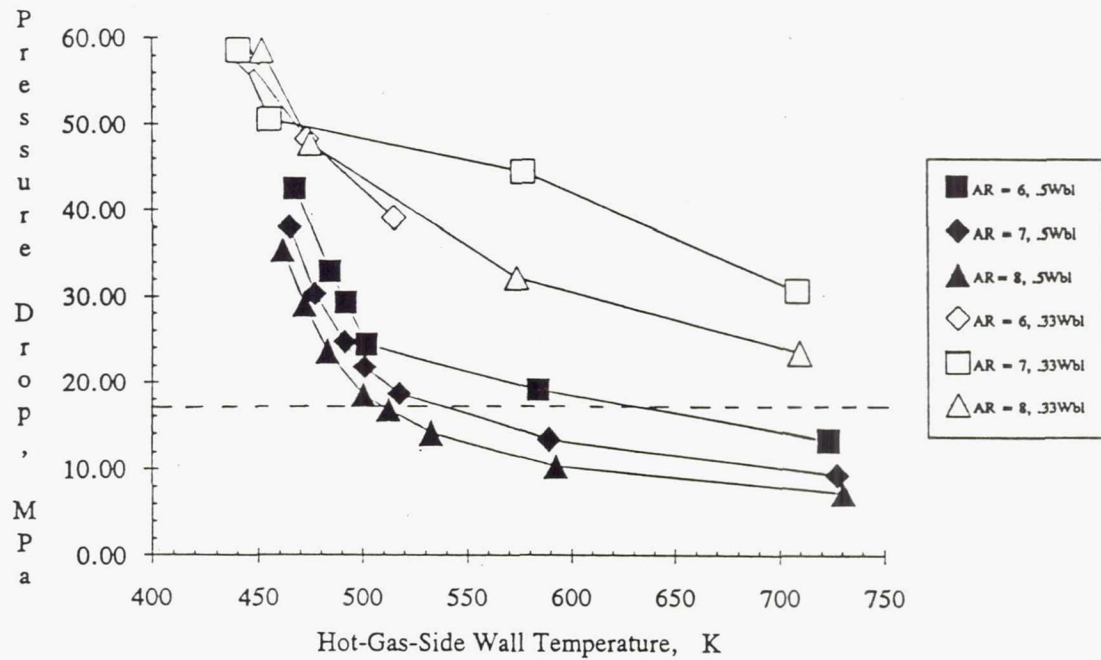
Figure 30.   Pressure Drop and Wall Temperature Values for Aspect
Ratios from 6 to 8 at Half the Baseline Width and One
Third the Baseline Width (Carbon Monoxide Cooling).
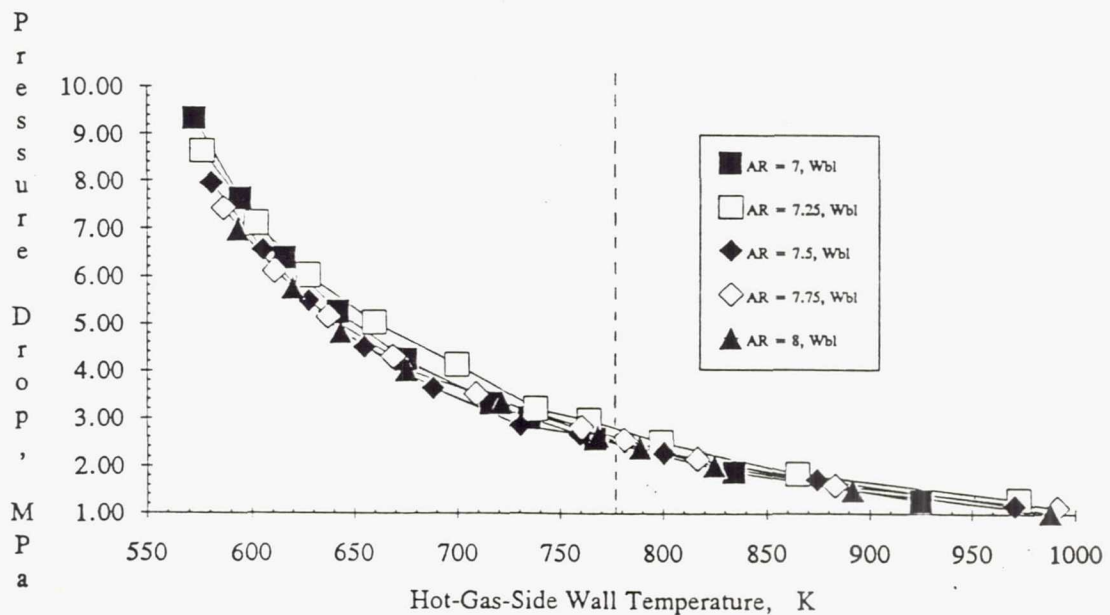
Figure 31.   Pressure Drop and Wall Temperature Values for Aspect
Ratios of 7.0, 7.25, 7.5, 7.75, and 8. at the Baseline
Width. (Carbon Monoxide Cooling).

58

and 1.2 were then evaluated, as shown in Figure 32. Although the data is very close for each case, an aspect ratio of 7.5 and the baseline width seemed to still be the optimum configuration. For a flowrate of 63.5 kg/sec (140.0 lbm/sec), the pressure drop is 3.63 MPa (527 psia) and the maximum hot-gas-side wall temperature is 688 K (1239 °R).
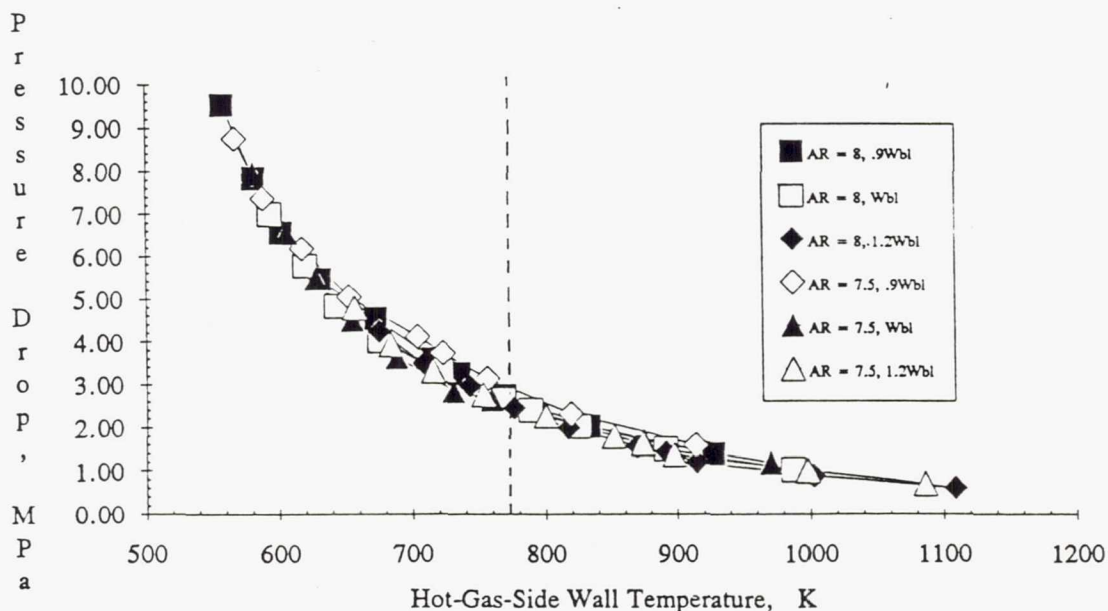
Figure 32. Pressure Drop and Wall Temperature Values for an Aspect Ratio of 7.5 and 8.0 and Widths of .9 and 1.2 of the Baseline Width (Carbon Monoxide Cooling).

CHAPTER VIII

DISCUSSION OF RESULTS

Two different fluids, oxygen and carbon monoxide, were evaluated as coolants for rocket engines used for a manned mission to Mars. Supercritical oxygen cooling, the first option, has been experimentally and analytically tested with kerosene/oxygen combustion and is capable of cooling rocket engine chambers such that the wall material does not reach the plastic region (ref. 32 - 34). Supercritical carbon monoxide, the second option, has only recently been considered as a regenerative coolant, and hence, this is the first research to study carbon monoxide as a coolant. Both concepts were evaluated for their heat transfer and fluid flow characteristics and were found to be potentially viable as cooling candidates. The property comparison indicated that it cannot be determined explicitly which fluid is a better coolant. The Prandtl Number for carbon monoxide was up to 16% higher than oxygen, while the nondimensionalized density of oxygen was 10% above carbon monoxide.

Heat transfer correlations were examined for applicability to each concept and a correlation was chosen for each coolant. Implementing the heat transfer correlations in the Rocket Engine Heat Transfer Evaluation Program (REHTEP), the two coolants were compared and the coolant

geometries were optimized for each option. The REHTEP was validated with experimental data for liquid oxygen cooling and this validation was extended to carbon monoxide cooling, for which no experimental data is available.

The optimum coolant channel geometry is defined as that which gives the lowest pressure drop for a given hot-gas-side wall temperature, within the pressure drop and temperature constraints mentioned previously. The thrust chamber contour was determined from the Rao Method of Optimization (ref. 10) and equations from ref. 11.

Oxygen Cooling Results

As mentioned in the previous chapter, various coolant channel geometries were analyzed with oxygen cooling using REHTEP. Because the optimum configuration was very close to the temperature limitation of the chamber material, a second configuration is also discussed for oxygen cooling.

The optimum coolant channel geometry for oxygen is given in Table VII. The regeneratively cooled section of the chamber is shown in Figure 33. This geometry has 292 channels at the throat which have an aspect ratio of 8 with a width of 0.594 mm (0.0234 in.). In the cylindrical combustion section, the optimum geometry has 584 channels with a width of 0.884 mm (.0343 in.) and an aspect ratio of 8. Due to manufacturing constraints, the number of cooling channels could only be doubled, tripled, quadrupled, etc. Therefore, the width of the cooling channels was not kept constant over the entire length of the thrust chamber. Instead, it varied from location to location in an effort to keep the channel width roughly equal to the distance between coolant channels while keeping the number of cooling channels consistent. The number of

Table VII. Optimum Cooling Channel Configuration for Oxygen.

Distance	Contour Diameter	Cooling Channel Width	Cooling Channel Height	Cooling Channel Area	Number of Cooling Channels
cm	cm	cm	cm	cm^2	
-109.6	32.02	0.08839	0.7071	0.06250	584
-96.94	32.02	0.08839	0.7071	0.06250	584
-84.24	32.02	0.08839	0.7071	0.06250	584
-71.54	32.02	0.08839	0.7071	0.06250	584
-58.84	32.02	0.08839	0.7071	0.06250	584
-46.14	32.02	0.08839	0.7071	0.06250	584
-33.44	32.02	0.08839	0.7071	0.06250	584
-29.27	31.30	0.08534	0.6826	0.05827	584
-25.23	29.12	0.07925	0.6340	0.05024	584
-13.96	27.92	0.07620	0.6096	0.04645	584
-2.705	12.27	0.06706	0.5369	0.03597	292
-1.400	11.19	0.06096	0.4877	0.02973	292
0.000	10.82	0.05944	0.4755	0.02826	292
1.430	11.90	0.06401	0.5121	0.03278	292
1.632	12.26	0.06553	0.5243	0.03456	292
1.904	12.74	0.07010	0.5608	0.03932	292
3.162	15.06	0.08230	0.6584	0.05418	292
3.910	16.46	0.08839	0.7071	0.06250	292
5.734	19.91	0.1067	0.8534	0.09104	292
6.868	22.06	0.05944	0.4755	0.02826	584
8.202	24.56	0.06553	0.5243	0.03435	584
9.787	27.48	0.07315	0.5852	0.04281	584
13.92	34.83	0.09296	0.7437	0.06914	584
16.54	39.27	0.1036	0.8291	0.08592	584
19.41	43.98	0.1143	0.9144	0.1045	584

cooling channels was varied from 584 to 292 and back to 584 for the nozzle region. Bifurcation of the channels occurred 2.705 cm (1.065 in.) upstream of the throat and again 3.91 cm (1.539 in.) downstream of the throat. The regenerative cooled section ended 19.40 cm (7.640 in.) downstream of the throat although the total nozzle was 702.3 cm (276.5 in.) long. The remainder of the nozzle was sufficiently cooled with radiation cooling.

This configuration gives a coolant pressure drop of 6.46 MPa (937 psia) at the maximum flowrate of 50.97 kg/sec (112.4 lbm/sec) as shown in Table VIII. The maximum hot-gas side wall temperature under these conditions is 744 K (1340 R). At approximately the same temperature, the next best case has a coolant pressure drop of 7.37 MPa (1080 psia), also shown in Table VIII. However, the wall temperature for this optimum configuration is very close to the maximum allowable temperature of 778 K (1400. R), at the maximum available oxygen flow of 50.97 kg/sec (112.4 lbm/sec). The second case has a lower temperature at the maximum flowrate and, therefore, was chosen so that a larger margin of error would exist for the wall temperature results. This configuration gives a coolant pressure drop of 9.11 MPa (1320 psia) at the maximum flowrate of 50.97 kg/sec (112.4 lbm/sec). The maximum hot-gas side wall temperature under these conditions is 702 K (1264 R).

The second geometry has 318 channels at the throat which have an aspect ratio of 8 with a width of 0.546 mm (0.0215 in.). This geometry is shown in Table IX. In the cylindrical combustion section, there are 636 channels with a width of .810 mm (.0319 in.) and an aspect ratio of 8. The number of cooling channels was varied from 636 to 318 and back to 636 for the nozzle region.

DETAIL A-A
TYPICAL COOLING
CHANNEL SECTION

WIDTH
0.0594 cm

HEIGHT
0.4755 cm
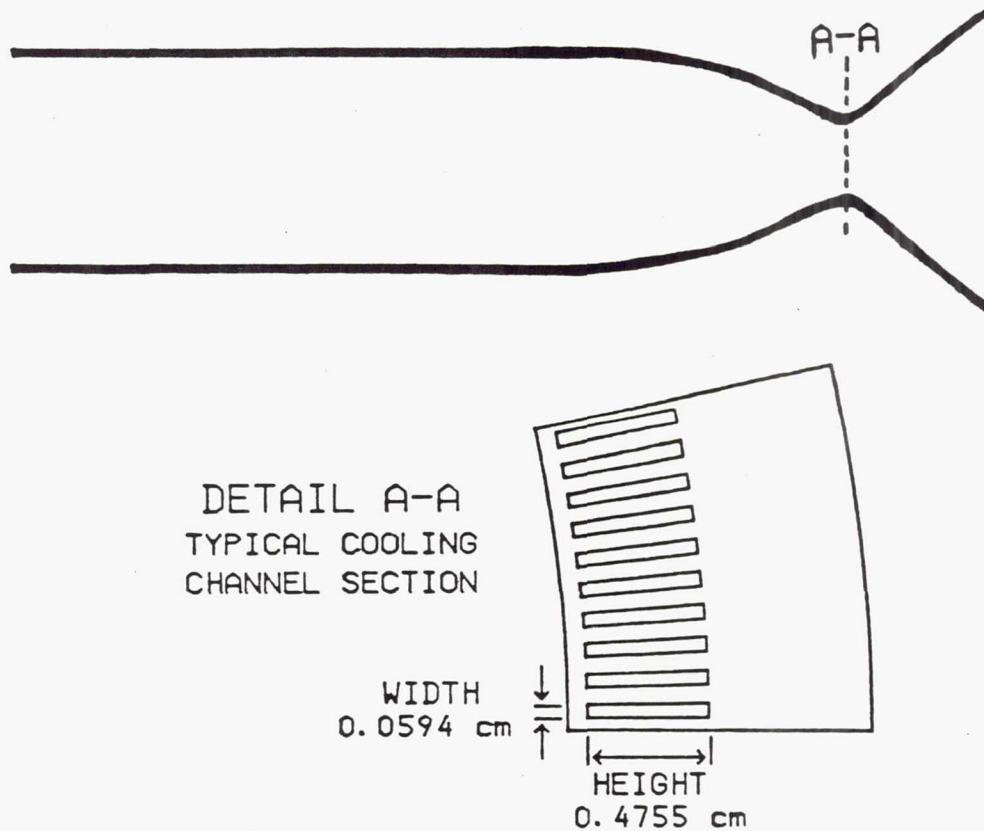
Figure 33. Regeneratively-Cooled Section of the Optimized Thrust
Chamber for Oxygen Cooling

Table VIII. REHTEP Results for the Two Best Configurations for Oxygen
Cooling.

Configuration	Flowrate (kg/s)	Wall Temp. (K)	Pressure Drop (MPa)
Aspect Ratio = 8	27.21	911	3.11
Width = .6 W_{bl}	36.29	828	4.29
(Oxygen Optimum)	45.36	769	5.56
	50.97	744	6.46
Aspect Ratio = 8	27.21	863	4.52
Width = .55 W_{bl}	36.29	786	6.08
(Second Oxygen)	45.36	727	7.85
	50.97	702	9.11

Table IX. Second Best Cooling Channel Configuration for Oxygen.

Distance	Contour Diameter	Cooling Channel Width	Cooling Channel Height	Cooling Channel Area	Number of Cooling Channels
cm	cm	cm	cm	cm^2	
-109.6	32.02	0.08103	0.6482	0.05252	636
-96.94	32.02	0.08103	0.6482	0.05252	636
-84.24	32.02	0.08103	0.6482	0.05252	636
-71.54	32.02	0.08103	0.6482	0.05252	636
-58.84	32.02	0.08103	0.6482	0.05252	636
-46.14	32.02	0.08103	0.6482	0.05252	636
-33.44	32.02	0.08103	0.6482	0.05252	636
-29.27	31.30	0.07823	0.6258	0.04896	636
-25.23	29.12	0.07264	0.5811	0.04222	636
-13.96	27.92	0.06985	0.5588	0.03903	636
-2.705	12.27	0.06147	0.4917	0.03022	318
-1.400	11.19	0.05588	0.4470	0.02498	318
0.000	10.82	0.05461	0.4359	0.02380	318
1.430	11.90	0.05867	0.4694	0.02754	318
1.632	12.26	0.06020	0.4806	0.02893	318
1.904	12.74	0.06426	0.5141	0.03304	318
3.162	15.06	0.07544	0.6035	0.04553	318
3.910	16.46	0.08103	0.6482	0.05252	318
5.734	19.91	0.09779	0.7823	0.07650	318
6.868	22.06	0.05461	0.4359	0.02380	636
8.202	24.56	0.06020	0.4806	0.02893	636
9.787	27.48	0.06706	0.5364	0.03597	636
13.92	34.83	0.08534	0.6817	0.05818	636
16.54	39.27	0.09500	0.7600	0.07219	636
19.41	43.98	0.1049	0.8382	0.08793	636

As can be seen in Table VIII, the results for these two configurations are similar. As was shown in Figures 25-28, many of the other configurations are outside of the temperature and pressure limits.

Carbon Monoxide Cooling Results

The optimum coolant channel geometry for carbon monoxide is given in Table X. This geometry has 175 channels at the throat which have an aspect ratio of 7.5 with a width of 0.991 mm (0.039 in.). In the cylindrical combustion section, the optimum geometry has 350 channels with a width of .884 mm (.0343 in.) and an aspect ratio of 7.5. The number of cooling channels was varied from 350 to 175 and back to 350 for the nozzle region. The regeneratively cooled section of the chamber is shown in Figure 34.

A-A

DETAIL A-A
TYPICAL COOLING
CHANNEL SECTION

WIDTH
0.0991 cm

HEIGHT
0.7430 cm
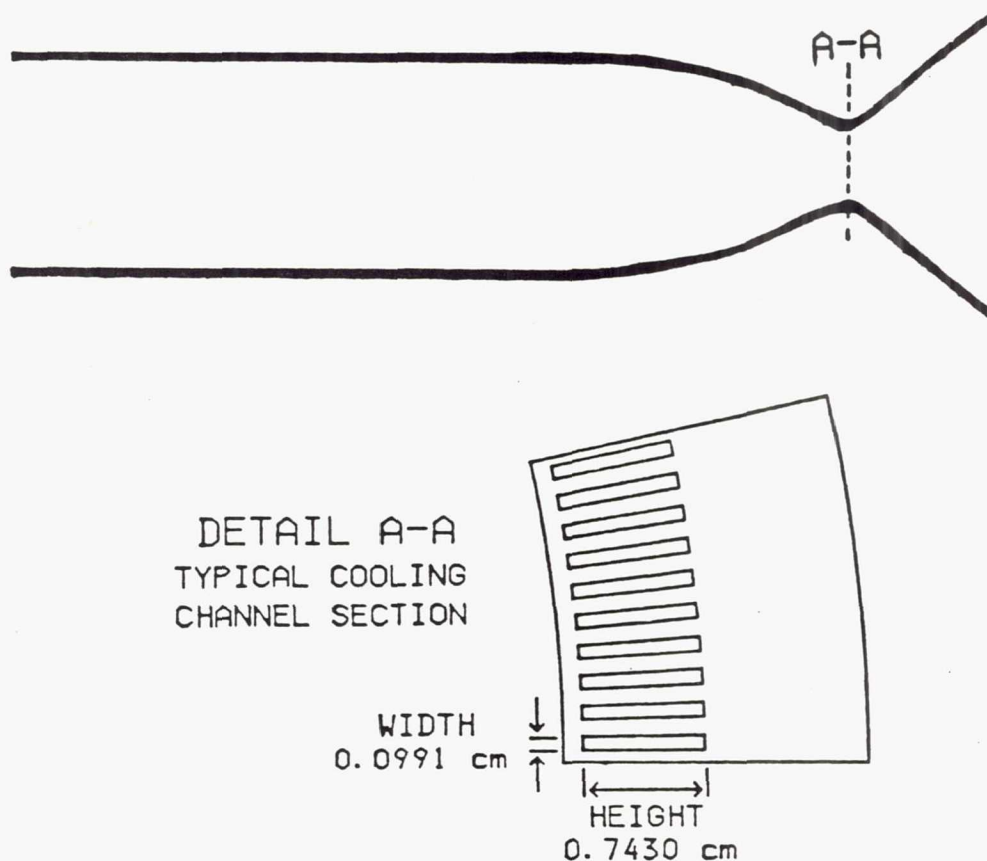
Figure 34. Regeneratively-Cooled Section of the Optimized Thrust Chamber for Carbon Monoxide Cooling

Table X. Optimum Cooling Channel Configuration for Carbon Monoxide.

Distance	Contour Diameter	Cooling Channel Width	Cooling Channel Height	Cooling Channel Area	Number of Cooling Channels
cm	cm	cm	cm	cm^2	
-109.6	32.02	0.1473	1.104	0.1627	350
-96.94	32.02	0.1473	1.104	0.1627	350
-84.24	32.02	0.1473	1.104	0.1627	350
-71.54	32.02	0.1473	1.104	0.1627	350
-58.84	32.02	0.1473	1.104	0.1627	350
-46.14	32.02	0.1473	1.104	0.1627	350
-33.44	32.02	0.1473	1.104	0.1627	350
-29.27	31.30	0.1422	1.066	0.1517	350
-25.23	29.12	0.1321	0.9907	0.1308	350
-13.96	27.92	0.1270	0.9525	0.1210	350
-2.705	12.27	0.1118	0.8385	0.09367	175
-1.400	11.19	0.1016	0.7620	0.07740	175
0.000	10.82	0.09906	0.7430	0.07360	175
1.430	11.90	0.1067	0.8002	0.08535	175
1.632	12.26	0.1092	0.8190	0.08948	175
1.904	12.74	0.1168	0.8760	0.1024	175
3.162	15.06	0.1372	0.1029	0.1411	175
3.910	16.46	0.1473	0.1105	0.1627	175
5.734	19.91	0.1778	0.1332	0.2370	175
6.868	22.06	0.09906	0.7430	0.07360	350
8.202	24.56	0.1092	0.8190	0.08943	350
9.787	27.48	0.1219	0.9142	0.1114	350
13.92	34.83	0.1549	1.162	0.1800	350
16.54	39.27	0.1727	1.295	0.2236	350
19.41	43.98	0.1905	1.429	0.2722	350

This configuration gives a coolant pressure drop of 7.96 MPa (1145 psia) at the maximum flowrate of 101.9 kg/sec (225.7 lbm/sec). The maximum hot-gas side wall temperature under these conditions is 581. K (1045 R). At a flowrate of 50.97 kg/sec (112.4 lbm/sec), the coolant pressure drop is 2.66 MPa (386 psia) and the wall temperature reaches 759 K (1367 R).

Overall Comparison

The previous results demonstrate that carbon monoxide and oxygen both can cool the chambers within the pressure drop and temperature constraints imposed upon them. However, at optimum conditions carbon monoxide cooling results in lower pressure drops for a given wall temperature, which indicates that it is a slightly better coolant than oxygen. With the optimum carbon-monoxide-cooling configuration, at a flowrate of 63.5 kg/sec (140.00 lbm/sec) the wall temperature reaches 731 K (1315 R), resulting in a coolant pressure drop of 2.85 MPa (414 psia), as shown in Table XI. At a similar temperature, 727 K (1309 R), the coolant pressure drop with the second-best oxygen-cooling configuration is 7.85 MPa (1138 psia), a threefold increase. This pressure drop variation between the two fluids is probably a result of the difference in their thermophysical properties.

When comparing the same configurations, such as an aspect ratio of 6 at the baseline width, the oxygen-cooling pressure drop is generally lower than the carbon-monoxide-cooling pressure drop at a given flowrate. Generally, the carbon monoxide cooling results in a lower pressure drop for a given wall temperature for a given configuration, as well. However, this is not always true, as shown in Table XI. At an aspect ratio of 8 at $.333w_{bl}$, the oxygen cooling results in both a lower

Table XI. REHTEP Results for Carbon Monoxide and Oxygen Cooling.

Configuration	Flowrate (kg/s)	Wall Temp. (K)	Pressure Drop (MPa)
Aspect Ratio = 8	27.21	911	3.11
Width = .6 W_{bl}	36.29	828	4.29
(Oxygen Optimum)	45.36	769	5.56
	50.97	744	6.46
Aspect Ratio = 7.5	27.21	971	1.18
Width = W_{bl}	36.29	874	1.72
(Carbon Monoxide	45.36	801	2.28
Optimum)	50.97	759	2.66
Aspect Ratio = 6	27.21	1160	1.25
Width = W_{bl}	36.29	1051	1.79
(Oxygen)	45.36	978	2.37
	50.97	947	2.75
Aspect Ratio = 6	27.21	885	1.76
Width = W_{bl}	36.29	796	2.58
(Carbon Monoxide)	45.36	739	3.54
	50.97	697	4.08
	101.9	542	12.82
Aspect Ratio = 6	27.21	737	10.38
Width = .5 W_{bl}	36.29	668	14.67
(Oxygen)	45.36	625	17.50
	50.97	605	21.22
Aspect Ratio = 6	27.21	724	13.39
Width = .5 W_{bl}	36.29	584	19.08
(Carbon Monoxide)	45.36	502	24.43
	50.97	492	29.25
Aspect Ratio = 8	27.21	636	17.84
Width = .33 W_{bl}	36.29	584	25.66
(Oxygen)	45.36	551	33.94
	50.97	540	38.56
Aspect Ratio = 8	27.21	710	23.51
Width = .33 W_{bl}	36.29	574	32.16
(Carbon Monoxide)	45.36	475	47.67
	50.97	452	58.61

temperature and a lower pressure drop at a flowrate of 27.21 kg/sec (60.0 lbm/sec). This indicates that under certain non-optimum conditions oxygen cooling is a better coolant.

The optimum cooling configuration is different for each fluid because of thermophysical property variations. It is not obvious from their properties which fluid would be a better coolant. The fluids' properties vary as the operating conditions (e.g. flowrate, inlet pressure, exit coolant temperature) vary, such that it cannot be generally stated that carbon monoxide is a better coolant than oxygen under all conditions. Carbon monoxide has a slightly wider range for which it is the better coolant. This allows more flexibility when designing a regeneratively-cooled rocket engine. Hence, carbon monoxide is determined to be the better coolant for a pump-fed, high-pressure propulsion system that uses in-situ propellants. Carbon monoxide cooling provides the mechanism to transfer enough heat from the combustion gases to keep the wall material in its elastic region.

CHAPTER IX

CONCLUSIONS

Regenerative cooling was evaluated for an in-situ propellant rocket engine to be used on the ascent/descent vehicle for a manned Mars mission. Supercritical oxygen and supercritical carbon monoxide were compared analytically to determine the best coolant. The thermophysical properties of the fluids were compared to determine the similarities of the two fluids. This comparison demonstrated that the density, viscosity, and conductivity were similar for the two fluids. However, the specific heat varies considerably between the two fluids. Therefore, different heat transfer correlations were chosen for carbon monoxide and oxygen, which were used to evaluate their heat transfer characteristics. Although an extensive literature search was undertaken to find appropriate correlations, other heat transfer correlations may be available that may more accurately predict the heat transfer characteristics of these two fluids.

Before the fluids could be compared to determine the best coolant, the rocket thrust chamber contour was optimized for the best engine performance. Using the optimized contour ensured that the fluids were evaluated for a heat flux that represents actual operating conditions. The fluids are evaluated not only for the same combustion conditions but

also for the same geometry configuration.

The rocket engine heat transfer evaluation program (REHTEP) was used to evaluate the thrust chamber heat transfer characteristics. The REHTEP was validated with experimental data for liquid oxygen cooling and this validation was extended to liquid carbon monoxide cooling. It has been used extensively to evaluate liquid oxygen cooling results for experimental research.

To determine which fluid is the better coolant, each fluid's cooling ability was evaluated for various coolant-channel geometry configurations. The REHTEP was used to determine the coolant pressure drop and hot-gas-side wall temperature. Low wall temperature and low pressure drop are characteristics of a good coolant.

Analytical results using the REHTEP indicated that carbon monoxide was a better coolant than oxygen, resulting in a threefold reduction in the pressure drop of the coolant through the cooling channels for a given hot-gas-side wall temperature, assuming optimal configurations for each. The optimum coolant channel configuration is defined as that which gives the lowest pressure drop for a given hot-gas-side wall temperature.

For the same geometry configuration, carbon monoxide generally resulted in a higher coolant pressure drop while maintaining a lower hot-gas-side wall temperature. However, at certain non-optimum conditions, oxygen cooling resulted in both a lower temperature and a lower pressure drop. Nevertheless, it can be stated that carbon monoxide is a better coolant than oxygen under most conditions.

Many of the geometry configurations gave results that were within the temperature and pressure constraints when carbon monoxide was used as the coolant. However, fewer options resulted in wall temperatures and

pressure drops within their respective constraints when used with oxygen cooling. Carbon monoxide has a wider range for which it is a better coolant, which allows for more flexibility when designing a pump-fed, high-pressure propulsion system for a manned Mars mission.

Although carbon monoxide appears to be a better coolant than oxygen, no experimental data exists to verify this conclusion. Therefore, experimental testing should be initiated to investigate the validity of these results. Initially, heated tube tests should be conducted to determine the heat transfer characteristics of carbon monoxide. Then carbon monoxide should be used to cool a subscale combustion chamber to determine its heat capacity under actual operating conditions. If carbon monoxide demonstrates good cooling experimentally as demonstrated analytically, future CO/O_2-propelled rocket engines should use it as the regenerative coolant.

APPENDIX A

THERMOPHYSICAL PROPERTIES OF CARBON MONOXIDE AND OXYGEN

Table A-1. Actual Values of Thermophysical Properties of Carbon Monoxide.

Pressure - 2.096 MPa

Temperature (K)	Density (kg/m^3)	Specific Heat (KJ/kg-K)	Thermal Conductivity (W/m-K x10^6)	Dynamic Viscosity (kg/m-s x10^7)	Prandtl Number
73.09	827.2	2.219	4.020	21.82	1.205
79.73	800.7	2.190	3.794	17.46	1.008
86.38	772.8	2.190	3.564	14.07	0.865
93.02	743.0	2.202	3.330	11.44	0.757
99.67	711.0	2.236	3.091	9.391	0.679
106.3	675.5	2.320	2.840	7.762	0.634
112.9	634.4	2.516	2.567	6.427	0.630
119.6	582.3	3.040	2.246	5.257	0.711
122.139	556.3	3.496	2.096	4.811	0.803
122.139	90.26	2.625	4.174	96.73	6.083
126.2	80.20	2.073	4.110	97.11	4.897
132.9	69.98	1.708	4.116	99.27	4.120
139.5	63.08	1.532	4.128	102.2	3.793
146.2	57.87	1.428	4.188	105.4	3.594
152.8	53.72	1.357	4.270	108.8	3.458
159.5	50.30	1.306	4.365	112.4	3.362
166.1	47.40	1.269	4.469	115.9	3.291
172.8	44.87	1.235	4.583	119.5	3.220
179.4	42.67	1.214	4.702	123.0	3.177
186.0	40.70	1.193	4.825	126.6	3.131
192.7	38.94	1.177	4.955	130.2	3.091
199.3	37.35	1.164	5.087	133.7	3.059
206.0	35.91	1.151	5.222	137.2	3.024
212.6	34.58	1.139	5.358	140.6	2.988

Table A-1. Actual Values of Thermophysical Properties of Carbon
Monoxide (continued).

Pressure — 3.494 MPa

Temperature	Density	Specific Heat	Thermal Conductivity	Dynamic Viscosity	Prandtl Number
(K)	(kg/m³)	(KJ/kg-K)	(W/m-K x10⁶)	(kg/m-s x10⁷)	
73.09	829.5	2.206	40.43	2227.	0.938
79.73	803.5	2.177	38.19	1786.	0.786
86.38	776.2	2.173	35.93	1443.	0.674
93.02	747.3	2.177	33.65	1178.	0.588
99.67	716.5	2.198	31.33	970.8	0.525
106.3	682.9	2.257	28.94	806.9	0.486
112.9	645.2	2.395	26.40	674.3	0.472
119.6	600.2	3.713	23.58	562.5	0.499
126.2	539.9	3.542	20.11	458.3	0.623
132.9	382.1	29.07	12.64	257.5	4.570
139.5	137.5	2.922	5.426	121.2	0.504
146.2	115.7	2.114	5.137	118.7	0.377
152.8	102.5	1.792	5.038	119.3	0.327
159.5	93.21	1.616	5.019	121.0	0.301
166.1	86.03	1.507	5.045	123.4	0.284
172.8	80.23	1.428	5.097	126.0	0.272
179.4	75.41	1.369	5.170	128.9	0.263
186.0	71.28	1.323	5.256	131.9	0.256
192.7	67.69	1.290	5.353	135.0	0.251
199.3	64.54	1.260	5.457	138.1	0.246
206.0	61.73	1.235	5.569	141.3	0.242
212.6	59.20	1.218	5.685	144.5	0.239

Pressure — 4.850 MPa

Temperature	Density	Specific Heat	Thermal Conductivity	Dynamic Viscosity	Prandtl Number
(K)	(kg/m³)	(KJ/kg-K)	(W/m-K x10⁶)	(kg/m-s x10⁷)	
73.09	831.7	2.198	40.63	2271.	12.29
79.73	806.1	2.165	38.43	1825.	10.28
86.38	779.4	2.156	36.21	1479.	8.809
93.02	751.3	2.156	33.98	1210.	7.682
99.67	721.5	2.169	31.73	1001.	6.843
106.3	689.4	2.206	29.43	835.9	6.268
112.9	654.2	2.307	27.03	703.3	6.003
119.6	613.8	2.533	24.45	593.7	6.150
126.2	564.5	2.994	21.54	498.0	6.920
132.9	495.4	4.011	17.86	402.8	9.045
139.5	352.9	8.784	11.61	239.2	18.10
146.2	212.4	4.233	7.286	156.0	9.062
152.8	169.1	2.667	6.374	141.0	5.900
159.5	146.2	2.119	6.019	136.6	4.807

Table A-1. Actual Values of Thermophysical Properties of Carbon
Monoxide (continued).

Pressure — 4.850 MPa (continued)

Temperature	Density	Specific Heat	Thermal Conductivity	Dynamic Viscosity	Prandtl Number
(K)	(kg/m³)	(KJ/kg-K)	(W/m-K x10⁶)	(kg/m-s x10⁷)	
166.1	131.0	1.842	5.855	135.6	4.266
172.8	119.8	1.675	5.786	136.1	3.941
179.4	111.0	1.562	5.772	137.6	3.722
186.0	103.9	1.478	5.793	139.5	3.559
192.7	97.85	1.415	5.838	141.7	3.436
199.3	92.70	1.369	5.902	144.2	3.346
206.0	88.20	1.331	5.980	146.8	3.270
212.6	84.21	1.298	6.068	149.6	3.199

Pressure — 6.289 MPa

Temperature	Density	Specific Heat	Thermal Conductivity	Dynamic Viscosity	Prandtl Number
(K)	(kg/m³)	(KJ/kg-K)	(W/m-K x10⁶)	(kg/m-s x10⁷)	
73.09	833.9	2.186	40.85	2318.	12.40
79.73	808.9	2.156	38.67	1867.	10.41
86.38	782.7	2.144	36.50	1517.	8.910
93.02	755.3	2.140	34.32	1245.	7.762
99.67	726.6	2.140	32.13	1033.	6.879
106.3	695.9	2.165	29.91	866.0	6.267
112.9	662.7	2.236	27.63	732.7	5.928
119.6	625.8	2.407	25.25	624.0	5.950
126.2	583.1	2.717	22.67	532.1	6.378
132.9	530.6	3.153	19.75	449.4	7.173
139.5	459.2	3.940	16.17	365.9	8.916
146.2	357.6	4.966	11.92	246.9	10.283
152.8	267.8	3.894	8.984	190.2	8.243
159.5	217.8	2.851	7.707	166.8	6.173
166.1	188.0	2.307	7.103	157.0	5.099
172.8	167.9	1.993	6.781	152.6	4.486
179.4	153.1	1.796	6.604	151.0	4.105
186.0	141.5	1.662	6.511	150.8	3.849
192.7	132.1	1.566	6.473	151.5	3.665
199.3	124.3	1.491	6.471	152.8	3.520
206.0	117.6	1.432	6.497	154.5	3.405
212.6	111.8	1.386	6.544	156.5	3.314

Table A-1.   Actual Values of Thermophysical Properties of Carbon
             Monoxide (continued).

Pressure — 7.685 MPa

Temperature	Density	Specific Heat	Thermal Conductivity	Dynamic Viscosity	Prandtl Number
(K)	(kg/m³)	(KJ/kg-K)	(W/m-K x10⁶)	(kg/m-s x10⁷)	
73.09	836.1	2.177	41.05	2363.	12.53
79.73	811.4	2.144	38.91	1908.	10.51
86.38	785.8	2.131	36.77	1554.	9.006
93.02	759.1	2.123	34.63	1278.	7.836
99.67	731.2	2.119	32.50	1063.	6.933
106.3	701.7	2.127	30.35	894.7	6.270
112.9	670.2	2.186	28.17	760.3	5.899
119.6	635.8	2.320	25.92	651.5	5.830
126.2	597.4	2.558	23.56	561.2	6.094
132.9	552.9	2.818	21.02	483.3	6.479
139.5	499.1	3.107	18.17	412.0	7.045
146.2	432.2	3.576	15.04	308.3	7.329
152.8	356.9	3.735	12.04	250.5	7.773
159.5	293.4	3.245	9.932	210.2	6.866
166.1	249.4	2.692	8.723	187.6	5:790
172.8	219.1	2.294	8.030	175.5	5.014
179.4	197.1	2.031	7.619	168.9	4.503
186.0	180.4	1.846	7.366	165.5	4.148
192.7	167.1	1.712	7.212	163.9	3.892
199.3	156.3	1.612	7.124	163.5	3.700
206.0	147.1	1.537	7.082	163.9	3.556
212.6	139.3	1.474	7.075	164.8	3.434

Table A-2. Actual Values of Thermophysical Properties of Oxygen.

Pressure - 3.025 MPa

Temperature (K)	Density (kg/m³)	Specific Heat (KJ/kg-K)	Thermal Conductivity (W/m-K x10⁶)	Dynamic Viscosity (kg/m-s x10⁷)	Prandtl Number
85.02	1172.	1.74	4.69	24.01	1.13
92.74	1135.	1.75	3.53	19.51	0.96
100.47	1096.	1.73	3.37	16.01	0.82
108.2	1054.	1.74	3.20	13.26	0.72
115.9	1009.	1.79	3.03	11.06	0.65
123.7	960.2	1.90	2.84	9.27	0.62
131.4	902.5	2.09	2.62	7.77	0.62
139.1	828.6	2.52	2.36	6.42	0.69
141.90	793.7	2.88	2.24	5.92	0.76
141.90	129.5	2.46	5.26	131.2	6.14
146.8	114.1	1.88	5.16	131.5	4.79
154.6	99.41	1.53	5.15	134.2	3.99
162.3	89.56	1.36	5.15	137.9	3.63
170.0	82.19	1.26	5.22	142.0	3.42
177.8	76.31	1.19	5.31	146.2	3.27
185.5	71.46	1.14	5.42	150.6	3.16
193.2	67.34	1.11	5.54	155.0	3.09
201.0	63.77	1.08	5.67	159.3	3.02
208.7	60.63	1.06	5.82	163.7	2.97
216.4	57.86	1.04	5.96	168.0	2.93
224.1	55.36	1.03	6.11	172.3	2.89
231.9	53.10	1.01	6.27	176.6	2.85
239.6	51.03	1.00	6.43	180.8	2.82
247.3	49.16	1.00	6.60	184.9	2.79

Pressure - 5.045 MPa

Temperature (K)	Density (kg/m³)	Specific Heat (KJ/kg-K)	Thermal Conductivity (W/m-K x10⁶)	Dynamic Viscosity (kg/m-s x10⁷)	Prandtl Number
85.02	1175.	1.73	37.08	2457.	11.49
92.74	1139.	1.74	35.52	2001.	9.79
100.47	1101.	1.72	33.95	1645.	8.32
108.2	1061.	1.72	32.33	1366.	7.27
115.9	1018.	1.76	30.63	1144.	6.57
123.7	971.5	1.85	28.83	963.9	6.17
131.4	918.5	1.98	26.85	815.2	6.02
139.1	855.2	2.24	24.57	687.0	6.26
146.8	770.0	2.88	21.64	564.7	7.52
154.6	498.8	4.15	13.38	308.7	9.57
162.3	196.5	2.66	6.82	163.1	6.36
170.0	164.7	1.88	6.45	159.4	4.66

Table A-2. Actual Values of Thermophysical Properties of
Oxygen (Continued).

Pressure — 5.045 MPa (continued)

Temperature	Density	Specific Heat	Thermal Conductivity	Dynamic Viscosity	Prandtl Number
(K)	(kg/m³)	(KJ/kg-K)	(W/m-K x10⁶)	(kg/m-s x10⁷)	
177.8	145.9	1.58	6.31	159.9	4.01
185.5	132.6	1.42	6.28	161.9	3.65
193.2	122.4	1.31	6.30	164.7	3.44
201.0	114.2	1.24	6.36	168.0	3.28
208.7	107.3	1.19	6.44	171.4	3.16
216.4	101.5	1.15	6.54	175.0	3.08
224.1	96.36	1.12	6.65	178.7	3.00
231.9	91.86	1.09	6.78	182.5	2.94
239.6	87.86	1.08	6.91	186.2	2.90
247.3	84.25	1.06	7.05	190.0	2.86

Pressure — 7.060 MPa

Temperature	Density	Specific Heat	Thermal Conductivity	Dynamic Viscosity	Prandtl Number
(K)	(kg/m³)	(KJ/kg-K)	(W/m-K x10⁶)	(kg/m-s x10⁷)	
85.02	1179.	1.73	37.26	2512.	11.63
92.74	1143.	1.73	35.73	2050.	9.92
100.47	1106.	1.70	34.19	1690.	8.42
108.2	1068.	1.70	32.61	1407.	7.33
115.9	1026.	1.73	30.98	1181.	6.59
123.7	981.7	1.80	29.26	999.7	6.15
131.4	932.3	1.91	27.41	851.0	5.93
139.1	875.7	2.08	25.36	725.7	5.95
146.8	806.6	2.40	22.96	614.3	6.42
154.6	710.7	3.20	19.79	502.1	8.13
162.3	520.7	6.70	14.12	329.3	15.62
170.0	313.7	4.00	9.24	213.0	9.22
177.8	245.7	2.44	8.04	190.0	5.76
185.5	211.3	1.90	7.58	183.2	4.58
193.2	188.9	1.63	7.37	181.4	4.01
201.0	172.5	1.47	7.27	181.7	3.67
208.7	159.8	1.36	7.24	183.1	3.44
216.4	149.4	1.29	7.26	185.2	3.28
224.1	140.7	1.23	7.31	187.8	3.16
231.9	133.3	1.19	7.38	190.7	3.07
239.6	126.8	1.16	7.46	193.7	3.00
247.3	121.0	1.13	7.56	196.9	2.93

Table A-2. Actual Values of Thermophysical Properties of
            Oxygen (Continued).

Pressure - 9.077 MPa

Temperature	Density	Specific Heat	Thermal Conductivity	Dynamic Viscosity	Prandtl Number
(K)	(kg/m³)	(KJ/kg-K)	(W/m-K x10⁶)	(kg/m-s x10⁷)	
85.02	1183.	1.72	37.44	2569.	11.81
92.74	1148.	1.72	35.94	2100.	10.05
100.47	1111.	1.70	34.43	1734.	8.54
108.2	1074.	1.68	32.89	1447.	7.40
115.9	1034.	1.71	31.30	1218.	6.65
123.7	991.1	1.76	29.66	1034.	6.15
131.4	944.5	1.85	27.91	885.1	5.87
139.1	892.6	1.98	26.02	760.8	5.78
146.8	832.5	2.18	23.91	654.0	5.95
154.6	758.8	2.52	21.44	556.5	6.55
162.3	659.4	3.24	18.25	457.1	8.11
170.0	519.1	4.15	14.24	333.5	9.71
177.8	389.1	3.49	11.09	256.6	8.07
185.5	313.8	2.57	9.58	223.4	5.99
193.2	269.6	2.05	8.85	209.3	4.85
201.0	240.1	1.75	8.46	203.0	4.21
208.7	218.7	1.57	8.25	200.4	3.81
216.4	202.0	1.45	8.13	199.7	3.56
224.1	188.5	1.36	8.08	200.3	3.37
231.9	177.3	1.29	8.08	201.6	3.23
239.6	167.7	1.24	8.10	203.5	3.12
247.3	159.4	1.20	8.16	205.7	3.03

Pressure - 11.09 MPa

Temperature	Density	Specific Heat	Thermal Conductivity	Dynamic Viscosity	Prandtl Number
(K)	(kg/m³)	(KJ/kg-K)	(W/m-K x10⁶)	(kg/m-s x10⁷)	
85.02	1187.	1.72	37.62	2625.	11.98
92.74	1152.	1.71	36.14	2149.	10.18
100.47	1116.	1.68	34.66	1779.	8.64
108.2	1080.	1.67	33.15	1487.	7.49
115.9	1041.	1.69	31.60	1255.	6.70
123.7	999.7	1.73	30.02	1069.	6.17
131.4	955.5	1.80	28.36	917.9	5.84
139.1	907.1	1.90	26.60	793.5	5.67
146.8	852.9	2.04	24.68	688.7	5.69
154.6	790.3	2.24	22.56	597.0	5.94
162.3	715.0	2.56	20.08	512.3	6.54
170.0	622.1	2.99	17.25	412.0	7.14
177.8	517.2	3.19	14.36	337.3	7.49
185.5	425.5	2.87	12.14	282.7	6.68

Table A-2. Actual Values of Thermophysical Properties of
            Oxygen (Continued).

Pressure — 11.09 MPa (continued)

Temperature	Density	Specific Heat	Thermal Conductivity	Dynamic Viscosity	Prandtl Number
(K)	(kg/m^3)	(KJ/kg-K)	(W/m-K x10^6)	(kg/m-s x10^7)	
193.2	360.0	2.40	10.77	251.0	5.60
201.0	315.0	2.04	9.96	233.8	4.79
208.7	282.7	1.79	9.47	224.4	4.24
216.4	258.3	1.62	9.17	219.3	3.86
224.1	239.1	1.49	8.99	216.8	3.59
231.9	223.4	1.40	8.88	215.8	3.41
239.6	210.2	1.33	8.83	215.9	3.26
247.3	198.9	1.28	8.82	216.8	3.14

Table A-3. Normalized Values of Thermophysical Properties of Carbon
Monoxide.

Pressure Ratio — 0.60

T/T(crit)	Rho/Rho(crit)	C_p/C_p(crit)	k/k(crit)	μ/μ(crit)
0.55	2.16	0.08	0.32	0.08
0.60	2.10	0.08	0.30	0.07
0.65	2.02	0.08	0.28	0.05
0.70	1.94	0.08	0.26	0.04
0.75	1.86	0.08	0.24	0.04
0.80	1.77	0.08	0.22	0.03
0.85	1.66	0.09	0.20	0.02
0.90	1.52	0.10	0.18	0.02
0.95	0.21	0.07	0.33	0.38
1.00	0.18	0.06	0.33	0.39
1.05	0.17	0.05	0.33	0.40
1.10	0.15	0.05	0.33	0.41
1.15	0.14	0.04	0.34	0.42
1.20	0.13	0.04	0.35	0.44
1.25	0.12	0.04	0.35	0.45
1.30	0.12	0.04	0.36	0.46
1.35	0.11	0.04	0.37	0.48
1.40	0.11	0.04	0.38	0.49
1.45	0.10	0.04	0.39	0.51
1.50	0.10	0.04	0.40	0.52
1.55	0.09	0.04	0.41	0.53
1.60	0.09	0.04	0.42	0.55

Pressure Ratio — 1.00

T/T(crit)	Rho/Rho(crit)	C_p/C_p(crit)	k/k(crit)	μ/μ(crit)
0.55	2.17	0.08	3.20	8.65
0.60	2.10	0.07	3.02	6.94
0.65	2.03	0.07	2.84	5.61
0.70	1.96	0.07	2.66	4.57
0.75	1.88	0.08	2.48	3.77
0.80	1.79	0.08	2.29	3.13
0.85	1.69	0.08	2.09	2.62
0.90	1.57	0.09	1.87	2.18
0.95	1.41	0.12	1.59	1.78
1.00	1.00	1.00	1.00	1.00
1.05	0.36	0.10	0.43	0.47
1.10	0.30	0.07	0.41	0.46
1.15	0.27	0.06	0.40	0.46
1.20	0.24	0.06	0.40	0.47
1.25	0.23	0.05	0.40	0.48
1.30	0.21	0.05	0.40	0.49
1.35	0.20	0.05	0.41	0.50
1.40	0.19	0.05	0.42	0.51
1.45	0.18	0.04	0.42	0.52

Table A-3. Normalized Values of Thermophysical Properties of Carbon
            Monoxide (Continued).

Pressure Ratio - 1.00 (continued)

T/T(crit)	Rho/Rho(crit)	C_p/C_p(crit)	k/k(crit)	μ/μ(crit)
1.50	0.17	0.04	0.43	0.54
1.55	0.16	0.04	0.44	0.55
1.60	0.15	0.04	0.45	0.56

Pressure Ratio - 1.40

T/T(crit)	Rho/Rho(crit)	C_p/C_p(crit)	k/k(crit)	μ/μ(crit)
0.55	2.18	0.08	3.22	8.82
0.60	2.11	0.07	3.04	7.09
0.65	2.04	0.07	2.87	5.74
0.70	1.97	0.07	2.69	4.70
0.75	1.89	0.07	2.51	3.89
0.80	1.80	0.08	2.33	3.25
0.85	1.71	0.08	2.14	2.73
0.90	1.61	0.09	1.94	2.31
0.95	1.48	0.10	1.70	1.93
1.00	1.30	0.14	1.41	1.56
1.05	0.92	0.30	0.92	0.93
1.10	0.56	0.15	0.58	0.61
1.15	0.44	0.09	0.50	0.55
1.20	0.38	0.07	0.48	0.53
1.25	0.34	0.06	0.46	0.53
1.30	0.31	0.06	0.46	0.53
1.35	0.29	0.05	0.46	0.53
1.40	0.27	0.05	0.46	0.54
1.45	0.26	0.05	0.46	0.55
1.50	0.24	0.05	0.47	0.56
1.55	0.23	0.05	0.47	0.57
1.60	0.22	0.04	0.48	0.58

Pressure Ratio - 1.80

T/T(crit)	Rho/Rho(crit)	C_p/C_p(crit)	k/k(crit)	μ/μ(crit)
0.55	2.18	0.08	3.23	9.00
0.60	2.12	0.07	3.06	7.25
0.65	2.05	0.07	2.89	5.89
0.70	1.98	0.07	2.72	4.83
0.75	1.90	0.07	2.54	4.01
0.80	1.82	0.07	2.37	3.36
0.85	1.73	0.08	2.19	2.85
0.90	1.64	0.08	2.00	2.42
0.95	1.53	0.09	1.79	2.07

Table A-3. Normalized Values of Thermophysical Properties of Carbon Monoxide (Continued).

Pressure Ratio - 1.80 (continued)

T/T(crit)	Rho/Rho(crit)	C_p/C_p(crit)	k/k(crit)	μ/μ(crit)
1.00	1.39	0.11	1.56	1.75
1.05	1.20	0.14	1.28	1.42
1.10	0.94	0.17	0.94	0.96
1.15	0.70	0.13	0.71	0.74
1.20	0.57	0.10	0.61	0.65
1.25	0.49	0.08	0.56	0.61
1.30	0.44	0.07	0.54	0.59
1.35	0.40	0.06	0.52	0.59
1.40	0.37	0.06	0.52	0.59
1.45	0.35	0.05	0.51	0.59
1.50	0.33	0.05	0.51	0.59
1.55	0.31	0.05	0.51	0.60
1.60	0.29	0.05	0.52	0.61

Pressure Ratio - 2.20

T/T(crit)	Rho/Rho(crit)	C_p/C_p(crit)	. k/k(crit)	μ/μ(crit)
0.55	2.19	0.07	3.25	9.18
0.60	2.12	0.07	3.08	7.41
0.65	2.06	0.07	2.91	6.03
0.70	1.99	0.07	2.74	4.96
0.75	1.91	0.07	2.57	4.13
0.80	1.84	0.07	2.40	3.47
0.85	1.75	0.08	2.23	2.95
0.90	1.66	0.08	2.05	2.53
0.95	1.56	0.09	1.86	2.18
1.00	1.45	0.10	1.66	1.88
1.05	1.31	0.11	1.44	1.60
1.10	1.13	0.12	1.19	1.20
1.15	0.93	0.13	0.95	0.97
1.20	0.77	0.11	0.79	0.82
1.25	0.65	0.09	0.69	0.73
1.30	0.57	0.08	0.64	0.68
1.35	0.52	0.07	0.60	0.66
1.40	0.47	0.06	0.58	0.64
1.45	0.44	0.06	0.57	0.64
1.50	0.41	0.06	0.56	0.63
1.55	0.39	0.05	0.56	0.64
1.60	0.36	0.05	0.56	0.64

Table A-4. Normalized Values of Thermophysical Properties of
Oxygen.

Pressure Ratio − 0.60

T/T(crit)	Rho/Rho(crit)	C_p/C_p(crit)	k/k(crit)	μ/μ(crit)
0.55	2.35	0.42	0.28	0.08
0.60	2.27	0.42	0.26	0.06
0.65	2.20	0.42	0.25	0.05
0.70	2.11	0.42	0.24	0.04
0.75	2.02	0.43	0.23	0.04
0.80	1.93	0.46	0.21	0.03
0.85	1.81	0.50	0.20	0.03
0.90	1.66	0.61	0.18	0.02
0.95	0.23	0.45	0.39	0.43
1.00	0.20	0.37	0.38	0.43
1.05	0.18	0.33	0.39	0.45
1.10	0.16	0.30	0.39	0.46
1.15	0.15	0.29	0.40	0.47
1.20	0.14	0.27	0.40	0.49
1.25	0.14	0.27	0.41	0.50
1.30	0.13	0.26	0.42	0.52
1.35	0.12	0.25	0.43	0.53
1.40	0.12	0.25	0.45	0.54
1.45	0.11	0.25	0.46	0.56
1.50	0.11	0.24	0.47	0.57
1.55	0.10	0.24	0.48	0.59
1.60	0.10	0.24	0.49	0.60

Pressure Ratio − 1.00

T/T(crit)	Rho/Rho(crit)	C_p/C_p(crit)	k/k(crit)	μ/μ(crit)
0.55	2.36	0.42	2.77	7.96
0.60	2.28	0.42	2.66	6.48
0.65	2.21	0.41	2.54	5.33
0.70	2.13	0.41	2.42	4.43
0.75	2.04	0.42	2.29	3.71
0.80	1.95	0.45	2.15	3.12
0.85	1.84	0.48	2.01	2.64
0.90	1.71	0.54	1.84	2.23
0.95	1.54	0.69	1.62	1.83
1.00	1.00	1.00	1.00	1.00
1.05	0.39	0.64	0.51	0.53
1.10	0.33	0.45	0.48	0.52
1.15	0.29	0.39	0.47	0.52
1.20	0.27	0.34	0.47	0.52
1.25	0.25	0.32	0.47	0.53
1.30	0.23	0.30	0.48	0.54
1.35	0.22	0.29	0.48	0.56
1.40	0.20	0.28	0.49	0.57
1.45	0.19	0.27	0.50	0.58

Table A-4. Normalized Values of Thermophysical Properties of
            Oxygen (Continued).

Pressure Ratio - 1.00 (Continued)

T/T(crit)	Rho/Rho(crit)	C_p/C_p(crit)	k/k(crit)	μ/μ(crit)
1.50	0.18	0.26	0.51	0.59
1.55	0.18	0.26	0.52	0.60
1.60	0.17	0.26	0.53	0.62

Pressure Ratio - 1.40

T/T(crit)	Rho/Rho(crit)	C_p/C_p(crit)	k/k(crit)	μ/μ(crit)
0.55	2.37	0.42	2.78	8.14
0.60	2.29	0.42	2.67	6.64
0.65	2.22	0.41	2.56	5.47
0.70	2.14	0.41	2.44	4.56
0.75	2.06	0.42	2.32	3.83
0.80	1.97	0.43	2.19	3.24
0.85	1.87	0.46	2.05	2.76
0.90	1.76	0.50	1.90	2.35
0.95	1.62	0.58	1.72	1.99
1.00	1.42	0.77	1.48	1.63
1.05	1.04	1.61	1.06	1.07
1.10	0.63	0.96	0.69	0.69
1.15	0.49	0.59	0.60	0.62
1.20	0.42	0.46	0.57	0.59
1.25	0.38	0.39	0.55	0.59
1.30	0.35	0.35	0.54	0.59
1.35	0.32	0.33	0.54	0.59
1.40	0.30	0.31	0.54	0.60
1.45	0.28	0.30	0.55	0.61
1.50	0.27	0.29	0.55	0.62
1.55	0.25	0.28	0.56	0.63
1.60	0.24	0.27	0.57	0.64

Pressure Ratio - 1.80

T/T(crit)	Rho/Rho(crit)	C_p/C_p(crit)	k/k(crit)	μ/μ(crit)
0.55	2.37	0.41	2.80	8.32
0.60	2.30	0.41	2.69	6.80
0.65	2.23	0.41	2.57	5.62
0.70	2.15	0.41	2.46	4.69
0.75	2.07	0.41	2.34	3.95
0.80	1.99	0.42	2.22	3.35
0.85	1.89	0.45	2.09	2.87
0.90	1.79	0.48	1.94	2.46
0.95	1.67	0.52	1.79	2.12

Table A-4. Normalized Values of Thermophysical Properties of
Oxygen (Continued).

Pressure Ratio - 1.80 (continued)

T/T(crit)	Rho/Rho(crit)	C_p/C_p(crit)	k/k(crit)	μ/μ(crit)
1.00	1.52	0.61	1.60	1.80
1.05	1.32	0.78	1.36	1.48
1.10	1.04	1.00	1.06	1.08
1.15	0.78	0.84	0.83	0.83
1.20	0.63	0.62	0.72	0.72
1.25	0.54	0.49	0.66	0.68
1.30	0.48	0.42	0.63	0.66
1.35	0.44	0.38	0.62	0.65
1.40	0.40	0.35	0.61	0.65
1.45	0.38	0.33	0.60	0.65
1.50	0.36	0.31	0.60	0.65
1.55	0.34	0.30	0.61	0.66
1.60	0.32	0.29	0.61	0.67

Pressure Ratio - 2.20

T/T(crit)	Rho/Rho(crit)	C_p/C_p(crit)	k/k(crit)	μ/μ(crit)
0.55	2.38	0.41	2.81	8.50
0.60	2.31	0.41	2.70	6.96
0.65	2.24	0.41	2.59	5.76
0.70	2.16	0.40	2.48	4.82
0.75	2.09	0.41	2.36	4.07
0.80	2.00	0.42	2.24	3.46
0.85	1.92	0.43	2.12	2.97
0.90	1.82	0.46	1.99	2.57
0.95	1.71	0.49	1.84	2.23
1.00	1.58	0.54	1.69	1.93
1.05	1.43	0.62	1.50	1.66
1.10	1.25	0.72	1.29	1.33
1.15	1.04	0.77	1.07	1.09
1.20	0.85	0.69	0.91	0.92
1.25	0.72	0.58	0.80	0.81
1.30	0.63	0.49	0.74	0.76
1.35	0.57	0.43	0.71	0.73
1.40	0.52	0.39	0.69	0.71
1.45	0.48	0.36	0.67	0.70
1.50	0.45	0.34	0.66	0.70
1.55	0.42	0.32	0.66	0.70
1.60	0.40	0.31	0.66	0.70

REFERENCES

1. Cordell, B.M.: Manned Mars Mission Overview. AIAA-89-2766, 1989. (25th Joint Propulsion Conference)

2. Von Braun, W.: The Mars Project. University of Illinois Press, Urbana, IL. 1953.

3. Ehricke, K.A.., et al.: A Study of Early Manned Interplanetary Missions- Final Summary Report. (AOK 63-0001) NASA Contract NAS8-5026, General Dynamics/Astronautics, San Diego, CA. 1963.

4. Sthulinger, E.; and King, J.C.: Concept for a Manned Mars Expedition with Electrically Propelled Vehicles. Prog. in Astron. & Aeron. vol.9, p.647 (1967).

5. Manned Mars Missions, Working Group Papers. M.B. Duke and P. W. Keaton, Eds. NASA-M002, 1986.

6. Galecki, D.L. : In-Situ Propellant Advantages for Fast Transfer to Mars. AIAA-88-2901, 1988 (24th Joint Propulsion Conference).

7. Palaszewski, B.; and Frisbee, R.: Advanced Propulsion for the Mars Rover Sample Return Mission. AIAA-88-2900, 24th Joint Propulsion Conference, 1988.

8. Frisbee, R.: Mass and Power Estimates for Mars In-Situ Propellant Production System. AIAA-87-1900, 1987.

9. McBride, B.S.; and Gordon, S.: Computer Program for Calculation of Complex Chemical Equilibrium Compositions, Rocket Performance, Incident and Reflected Shocks, and Chapman-Jouguet Detonations. NASA SP-279, 1971.

10. Nickerson, G.R.; Dang, A.L.; and Dunn,S.S.: The Rao Method Optimum Nozzle Contour Program. NAS8-36836 contract, 1988.

11. Huzel, D. K.; and Huang, D. H.: Design of Liquid Propellant Rocket Engines. NASA SP-125, 1971.

12. Fessler, T.E.: FLUID: A Numerical Interpolation Procedure for Obtaining Thermodynamic and Transport Properties of Fluids. NASA TMX-3572, 1972.

13. Ramohalli, K. et al.: Some Aspects of Space Propulsion with Extra-terrestrial Resources. J. of Spacecraft, vol. 24, no. 3, 1987.

14. Ash, R. et al.: Autonomous Oxygen Production for a Mars Return Vehicle. IAF-82-210, 1982.

15. Lawton, E.; and Frisbee, R.: A New Look at Oxygen Production on Mars: ISPP. JPL-D-2661, 1985 (Jet Propulsion Lab).

16. Lawton, E.: Risk Factors in the Development of Zirconia Cell Technology for the Production of Oxygen from the Martian Atmosphere. JPL-D-3549, 1986 (Jet Propulsion Lab).

17. Manned Mars Missions Summary Report. M.B. Duke and P.W. Keaton, Eds. NASA-M001, 1986.

18. Clapp, W.M.: Propellant Performance of Mars-Produced Carbon Monoxide. AIAA-86-1587, 1986.

19. Hill, P.G.; and Peterson, C.R.: Mechanics and Thermodynamics of Propulsion. Addison-Wesley Publishing Company; Reading, MA, 1965.

20. Fowler, J.R.: GASPLUS User's Manual. December, 1987.

21. Petukhov, B.S.: "Heat Transfer and Friction in Turbulent Pipe Flow with Variable Physical Properties", from Vol. 6: Advances in Heat Transfer, edited by J.P. Hartnett and T.F. Irvine, Academic Press, New York, 1970.

22. Dittus, F.W.; and Boelter, L.M.K.: Univ. Calif. Publs. Eng., Vol. 2, 1930, p.443.

23. McAdams, W.H.: Heat Transmissions. 3rd Edition, McGraw-Hill, New York, 1954.

24. Notter, R.H.; and Sleicher, C.A.: A Solution to the Turbulent Graetz Problem - III. Fully Developed and Entry Region Heat Transfer Rats. Chem. Eng. Sci., vol. 27, 1972, pp. 2073-2093.

25. Sieder, E.N.; and Tate, C.E.: Heat Transfer and Pressure Drop of Liquids in Tubes. Ind. Eng. Chem., Vol. 28, 1936, p. 1429.

26. Nusselt, W.: Der Wärmeaustausch zwischen Wand und Wasser in Rohr, Forsch. Geb. Ingenieurwes., Vol. 2, 1931, p. 309.

27. Spencer, R.G.; and Rousar, D.C.: Supercritical Oxygen Heat Transfer. NASA CR-135339, 1977.

28. Niino, M.; Kumakawa, A.; Yatsuyanagi, N.; and Suzuki, A.: "Heat Transfer for Characteristics of Liquid Hydrogen as a Coolant for the LO2/LH2 Rocket Thrust Chamber with the Channel Wall Construction," 18th. AIAA/SAE/ASME Joint Propulsion Conference, Cleveland, Ohio, June 21-23, 1982, AIAA paper 82-1107.

29. Kumakawa, A.; Niino, M.; Hendricks, R.C.; Giarratano, P.J.; and Arp, V.D.: "Volume-Energy Parameters for Heat Transfer to Supercritical Fluids," 15th International Symposium in Space Technology and Science, Tokyo, Japan, May 19-20, 1986, Proceeding Vol. 1, A87-2276 13-12, Tokyo,

30. Kumakawa, A.; Niino, M.; Hendricks, R.C.; Giarratano, P.J.; and Arp, V.D.: "Volume-Energy Parameters for Heat Transfer to Supercritical Fluids," 15th International Symposium in Space Technology and Science, Tokyo, Japan, May 19-20, 1986, Proceeding Vol. 1, A87-2276 13-12, Tokyo, AJNE Publishing Inc., 1986, pp. 389-399.

31. Hendricks, R.C.; Niino, M.; Kumakawa, A.; Yernshenko, V.M.; Yaskih, L.A.; Braun, M.J.; and Moullen, R.L.: "Friction Factors and Heat Transfer Coefficients for Hydrogen Systems Operating at Supercritical Pressures," Proceeding of Beijing International Symposium on Hydrogen Systems, Beijing, China, May 7-11, 1985.

32. Price, H.G.: Cooling of High-Pressure Rocket Thrust Chambers with Liquid Oxygen. J. Spacecraft and Rockets, Vol. 18, No. 4, 1981, pp. 338-343.

33. Price, H.G.; and Masters, P.A.: Liquid Oxygen Cooling of High Pressure LOX/Hydrocarbon Rocket Thrust Chambers. NASA TM-88805, 1986.

34. Armstrong, E.S.: Liquid Oxygen Cooling of Hydrocarbon Fueled Rocket Thrust Chambers. AIAA-89-2739, 1989.

35. Rao, G.V.R.: Exhaust Nozzle Contour for Optimum Thrust. Jet Propulsion, Vol. 28, June 1958.

36. Smith, J.P.: Systems Improved Numerical Differencing Analyzer (SINDA) User's Manual. April, 1971.

Report Documentation Page

1. Report No. NASA TM-103729 *Corrected Copy*	2. Government Accession No.	3. Recipient's Catalog No.

4. Title and Subtitle	5. Report Date
Cooling of In-Situ Propellant Rocket Engines for Mars Mission	January 1991
	6. Performing Organization Code

7. Author(s)	8. Performing Organization Report No.
Elizabeth S. Armstrong	E-5963
	10. Work Unit No. 590-21-21

9. Performing Organization Name and Address	11. Contract or Grant No.
National Aeronautics and Space Administration Lewis Research Center Cleveland, Ohio 44135-3191	
	13. Type of Report and Period Covered Technical Memorandum

12. Sponsoring Agency Name and Address	
National Aeronautics and Space Administration Washington, D.C. 20546-0001	14. Sponsoring Agency Code

16. Abstract

When contemplating the human exploration of Mars, many scenarios using various propulsion systems have been considered. One propulsion option of a Mars ascent/descent vehicle is multiple high-pressure, pump-fed rocket engines using in-situ propellants, which have been derived from substances available on the Martian surface. The chosen in-situ propellant combination for this analysis is carbon monoxide as the fuel and oxygen as the oxidizer. Both could be extracted from carbon dioxide, which makes up about 96% of the Martian atmosphere. A pump-fed rocket engine allows for higher chamber pressure than a pressure-fed engine, which in turn results in higher thrust and also higher heat flux in the combustion chamber. The heat flowing through the wall cannot be sufficiently dissipated by radiation cooling and, therefore, a regenerative coolant may be necessary to avoid melting the rocket engine. The two possible fluids for this coolant scheme, carbon monoxide and oxygen, are compared analytically. To determine their heat transfer capability, they are evaluated based upon their heat transfer and fluid flow characteristics. Heat transfer correlations were examined for applicability to each fluid and a correlation was chosen for each coolant. Implementing the heat transfer correlations into the Rocket Engine Heat Transfer Evaluation Program (REHTEP), the two coolants were compared and the coolant geometries were optimized while considering certain limitations such as temperature and pressure constraints. The pressure drop and hot-gas-side wall temperature results from REHTEP were compared for each coolant channel geometry to determine which fluid was the better coolant under optimum conditions. The use of carbon monoxide as a coolant results in a lower coolant inlet pressure from the turbopumps and a cooler chamber wall and, hence, a less severe operating condition. Overall, for a given flow rate and coolant pressure drop, carbon monoxide cooling results in lower wall temperatures than oxygen cooling, under optimum conditions.

17. Key Words (Suggested by Author(s))	18. Distribution Statement
Cooling; Oxygen; Carbon monoxide; Mars mission; Computer analysis; Heat transfer	Unclassified – Unlimited Subject Category 20

19. Security Classif. (of this report)	20. Security Classif. (of this page)	21. No. of pages	22. Price*
Unclassified	Unclassified	98	A05